Title
Slip-Based Coding of Local Shape and Texture in Mouse S1

Journal
Neuron, 97(2)

ISSN
0896-6273

Authors
Isett, Brian R
Feasel, Sierra H
Lane, Monet A
et al.

Publication Date
2018

DOI
10.1016/j.neuron.2017.12.021

Peer reviewed

HHS Public Access

Author manuscript

Neuron. Author manuscript; available in PMC 2019 January 17.

Published in final edited form as:

Neuron. 2018 January 17; 97(2): 418–433.e5. doi:10.1016/j.neuron.2017.12.021.

Slip-based coding of local shape and texture in mouse S1

Brian R. Isett, **Sierra H. Feasel**, **Monet A. Lane**, and **Daniel E. Feldman**[†]

Dept. of Molecular and Cellular Biology, and Helen Wills Neuroscience Institute, University of California Berkeley, Berkeley, CA 94720

Summary

Tactile objects have both local geometry (shape) and broader macroscopic texture, but how these different spatial scales are simultaneously encoded during active touch is unknown. In the whisker system, we tested for a shared code based on localized whisker micromotions (stick-slips) and slip-evoked spikes. We trained mice to discriminate smooth from rough surfaces, including ridged gratings and sandpaper. Whisker slips locked to ridges, and evoked temporally precise spikes (<10 ms jitter) in somatosensory cortex (S1) that could resolve ridges with ~1 mm accuracy. Slip-sensitive neurons also encoded touch and texture. On rough surfaces, both slip-evoked spikes and an additional non-slip signal elevated mean firing rate, allowing accurate rough-smooth texture decoding from population firing rate. 18% of neurons were selective among rough surfaces; thus, slips elicit spatially and temporally precise spiking in S1 that simultaneously encodes local shape (ridges) and is integrated into a macroscopic firing rate code for roughness.

eTOC Blurb

This study tests how local shape and texture are encoded during active whisker sensation. Local shape elicits stick-slip whisker motions and temporally precise spikes in somatosensory cortex. Spikes track local features and contribute to a firing rate code for roughness.

Keywords

neural coding; barrel cortex; texture; shape; spatial tuning; active sensation; virtual foraging; stick-slip; multiplexed code

Correspondence should be addressed to: Dept. of Molecular and Cell Biology, Helen Wills Neuroscience Institute, Univ. of California, Berkeley, Berkeley, CA 94720-3200, dfeldman@berkeley.edu.

[†]Lead Contact.

Declaration of Interests

The authors declare no competing interests.

Author Contributions

D.E.F. and B.R.I. conceived experiments, wrote the manuscript, and secured funding. B.R.I. designed hardware, performed experiments and analyzed data. B.R.I., S.H.I. and M.A.L. trained mice and analyzed behavior.

Introduction

Rodent whiskers, like human fingertips, are exquisitely sensitive to touch and extract precise information about object location, texture, and geometry (Brecht et al., 1997; Carvell and Simons, 1990; Diamond, 2010; Kleinfeld and Deschênes, 2011; Morita et al., 2011). The biomechanical basis and neural codes for these features are not completely understood, particularly during active sensation. A fundamental question is how discrete geometric features (local shapes) are represented simultaneously with macroscopic features like texture. During active whisker sensation, rodents rhythmically sweep the whiskers against objects, inducing whisker bends, vibrations and discrete high-velocity, high-acceleration micromotions called stick-slips, here termed “slips” (Chen et al., 2015; Diamond et al., 2008; O’Connor et al., 2010a; Wolfe et al., 2008; Zuo et al., 2011). Whisker slips are brief (~5 ms) spatially localized accelerations and decelerations of the whisker tip (Arabzadeh et al., 2005; Hires et al., 2013a; Wolfe et al., 2008) that evoke sparse, temporally precise spikes in S1 (Jadhav et al., 2009). Which tactile features are sensed by slips is only partially understood. In the “slip hypothesis” of texture encoding, higher friction on rough surfaces increases slip rate and amplitude, driving higher mean firing rate in S1 (Jadhav and Feldman, 2010; Zuo et al., 2015). This increase in time-averaged firing rate is hypothesized to encode roughness. However, other kinematic and mechanical features, such as whisker bend, may also contribute to roughness coding (Boubenec et al., 2014; Chen et al., 2015; Ewert et al., 2015) and whether slips and slip-evoked spikes are sufficiently robust to predict rough vs. smooth surfaces on a single-trial basis remains unknown.

We hypothesized that slips also play a role in coding local shape. In this model, slips occur more often when the moving whisker “bumps” over local surface irregularities, and slip-evoked spikes may therefore be an instantaneous (temporal) code for spatially precise surface features (Arabzadeh et al., 2005; Schwarz, 2016). If so, the same slips and slip-locked spikes could underlie both instantaneous coding of local spatial features, and coding of macroscopic texture by firing rate. Simultaneous temporal and rate codes have been recently observed in primate and rodent primary somatosensory cortex (Harvey et al., 2013; Zuo et al., 2015), but how these codes arise during active sensation is unknown.

To address these questions, we trained head-fixed mice to discriminate smooth from rough surfaces while running past surfaces on a virtual track. Rough stimuli consisted of raised gratings with 2–10 mm spatial period, and sandpaper. Active whisking and forward running generated complex sampling trajectories across surfaces. Slips and slip-evoked spikes were temporally precise and accumulated along ridges of raised gratings with ~ 1 mm spatial precision, recapitulating grating patterns. At the same time, time-averaged firing of individual units predicted rough vs. smooth trials with 85% accuracy. Both slip-evoked spikes and an additional, non-slip signal in slip-insensitive units contributed to this mean firing rate code for roughness. Thus, slips and slip-evoked spikes provide both an instantaneous signal for spatially localized features, and contribute to a slower firing rate signal that encodes macroscopic roughness.

Results

Mice discriminate Smooth vs. Rough surfaces on a virtual track

We trained head-fixed mice running on a passive disk treadmill to discriminate smooth from rough surface patches presented on a rotating cylinder (Figure 1). Surface patches were 3 cm long and consisted of a smooth surface, raised ridge gratings (2, 4, 8 or 10 mm spatial period), or coarse sandpaper (P150). Sandpaper and gratings were collectively termed "Rough" stimuli, as in past studies (Carvell and Simons, 1990; Morita et al., 2011; Zuo et al., 2015). Mice ran and actively whisked against the cylinder, which rotated in proportion to the mouse's running velocity, creating a 1D virtual track. Mice were trained in a Go/No-go task design to lick for water reward when they felt any of the Rough stimuli, and to withhold licking for Smooth stimuli. Training was performed in the dark, with stimuli only accessible by the whiskers. Thus, this was a virtual tactile foraging task in which mice were rewarded for finding rough patches along an otherwise smooth cylinder surface.

The task consisted of discrete trials which began when the cylinder, presenting a smooth surface, was translated medially to contact the whiskers (Figure 1B, static introduction). The mouse then self-initiated a trial by running forward, causing the stimulus cylinder to rotate proportional to run velocity (Figure 1B–C). This brought a randomly chosen stimulus patch, either smooth or rough, into whisker contact, and opened a 1.5–2 s response window in which mice licked or withheld licking to indicate choice. On Rough trials, licking above a threshold rate in the response window triggered water reward (Hit). On Smooth trials, licking was scored as a False Alarm (FA) and triggered a time out. No action was taken on Correct Rejection (CR) and Miss trials (Supplemental Movie 1). An example Hit trial is shown in Figure 1C. Cylinder rotation stopped when mice ran to the end of the stimulus patch. After the response window, the cylinder was retracted (inter-trial epoch). Rough and Smooth trials were presented in 50:50 ratio, and 7% of trials were catch trials in which the cylinder was translated only partially to the whiskers, so that the mouse whisked in air. Only C1 and C2 whiskers were intact. Multiple precautions ensured that mice solved the task using whisker tactile cues, and not auditory, visual or olfactory cues (STAR Methods).

During each trial, we imaged C1 and C2 whiskers in the rostrocaudal plane using a 1-dimensional CCD imaging system (4 kHz sampling rate). From this we calculated time series of whisker angle relative to the follicle and whisker contact position on the surface. We calculated the time and spatial position of first whisker contact with the leading edge of Rough stimuli (i.e., the onset of the first ridge or the P150 sandpaper), or with the corresponding position on the Smooth stimulus (Figure 1C). First contact was always by the C2 whisker, which is more rostral on the face. Substantial trial-to-trial variability in mouse locomotion and active whisking led to heterogeneous whisker exploration patterns across trials (Supplemental Movies 2–3). Calibration on a subset of trials using high-speed 2D imaging showed that our average error in estimating contact position was ~ 1 mm (Figure S1).

Mice were trained in stages until they reached criterion performance in discriminating rough and smooth trials with random, closed-loop stimulus presentation (>75% correct for 2 consecutive days). Training took 21 ± 13 sessions (n = 7 mice, Figure S2A) with all

whiskers intact, at which point all right whiskers except C1 and C2 were trimmed. Final discrimination was well above chance (78 ± 2.5% correct, 7 mice, total of 244 days above criterion), with significantly more licks to rough trials than smooth trials ($p < 0.001$, t-test; Figure 1D). This corresponded to a total d' of 1.63. All behavioral, whisker and neural data measurements were made in these 7 mice. There was no difference in Hit rate for individual Rough stimuli ($p = 0.48$, one-way ANOVA). However, Hit rate was weakly correlated with spatial frequency ($r^2 = 0.14$, $p= 0.038$; Figure 1D). Licks occurred 781 ± 29 ms after first contact on Hit trials (n = 1215 imaged trials), but were uniformly distributed in time on FA trials (Figure 1E). Mean running speed did not differ between Rough and Smooth trials ($p = 0.21$, paired t-test, Figure S2B–C). Thus, mice learned to discriminate rough and smooth surfaces in a closed-loop virtual track using two intact whiskers.

Whisker slip events are a potential cue for roughness

We first tested whether whisker slips could underlie discrimination of Rough vs. Smooth texture. Slips are known to correlate with roughness on sandpaper and irregular 2D surfaces (Ritt et al., 2008; Wolfe et al., 2008). We analyzed whisker slips and other whisker kinematics in a palpation window from 50 ms before First Contact to 200 ms before the first lick (Figure 2A). This truncation avoids contamination by licks and behavioral decision. We identified all slips defined by whisker acceleration above a ± 2.5 SD threshold in this window (Figure 2B). This threshold was chosen because slips > ± 2.5 SD maximally drive spikes in S1 single units (see below). Palpation window duration was 722 ± 454 ms (mean ± SD), and varied with running speed and lick time across trials. On non-lick trials, a 650 ms window was used.

We compared C2 whisker slip amplitude (absolute peak acceleration), slip rate, and mean speed (absolute whisker velocity) in the palpation window on Smooth vs. Rough trials. Smooth surfaces generated 28.3 ± 0.8 slips/s at a mean amplitude of 1.0 ± 0.01 °/ms^2 (n=3,355 Smooth trials; 29 imaging sessions in 7 mice). Collectively, rough surfaces generated 52.0 ± 1.2 slips/s at a mean amplitude of 1.2 ± 0.01 °/ms^2 in these same sessions (n=3,223 Rough trials). We z-scored slip rate and amplitude on all stimuli to Smooth data values in each mouse. Slip rate and amplitude significantly increased on Rough surfaces and decreased in air, relative to Smooth. Within Rough stimuli, slip rate and amplitude increased with spatial frequency, while mean whisker speed decreased (Figure 2C). The decrease in whisker speed was associated with reduced whisking amplitude (Figure S2D–E) but constant mean whisking frequency (18 ± 0.1 Hz; Figure S2F–G). Therefore, surface roughness was accompanied by increased slip rate and amplitude, as observed previously on sandpapers (Jadhav et al., 2009; Wolfe et al., 2008), but with decreased mean speed, due to lower whisk amplitude.

Because each whisk generates few slips, it has been unclear whether slips can accurately code roughness on a single-trial basis (Chen et al., 2015; Jadhav et al., 2009). To test this, we fit a GLM to classify Smooth and Rough stimuli based on C1 and C2 whisker slip rate and amplitude (STAR Methods). This model predicted stimulus identity on hold-out trials with 77.6 ± 11% accuracy (Figure 2D). This performance was significantly above chance (p

< 0.001, one-way t-test), and was not different from mouse behavioral discrimination accuracy (78 ± 4%) on the same trials (p = 0.91, paired t-test; Figure 2D).

To examine whether slips predict the mouse's behavioral decision to lick or not lick, we compared slip rate and amplitude during trials that elicited lick responses vs. trials with the same surfaces that elicited no licks. We found higher slip rate and slip amplitude during FA vs. CR trials on Smooth surfaces (Figure 2E, top). There was a similar trend for Hit vs. Miss trials on Rough surfaces. To examine whether this difference in whisker slips was sufficient to predict lick behavior, the slip GLM described above was refit to classify Lick and No-Lick trials. We then tested the model on slip data from held-out Hit, Miss, FA and CR trials. The model indeed predicted licks significantly more often on Hit than Miss trials, and on FA than CR trials (Figure 2E; Bottom). This suggests that trial-to-trial variability in slip sensory data biases lick responses, and that excess slips contribute to FA licks on Smooth trials. Thus, slips are a potent cue for roughness, and carry sufficient information to explain average mouse behavior and to accurately discriminate Smooth vs. Rough surfaces on single trials.

Slips cluster at ridges, providing a cue for local geometric features

How the whisker system detects specific local surface features, like ridges, is unknown. Because ridges are raised and have spatially sharp edges, they are likely to increase local whisker bend and the local coefficient of friction, which may increase the probability of stick-slip events. To test whether slips cluster at ridges, we plotted the prevalence of slips as a function of position of whisker contact on the stimulus surface (Figure 3A). Slips were spatially modulated and tended to cluster at the leading edge of ridges, and of the P150 sandpaper (Figure 3B). This was consistent across trials and mice (Figure 3B–C). Slips tracked the spatial period of gratings for 4–10 mm periods, but were less spatially precise for the 2 mm grating. This may be because the whisker often bent to span across two bars on the 2 mm grating, instead of separately contacting individual ridges (Figure S3A–B).

To confirm that ridges induce whisker acceleration transients, we calculated the ridge-triggered average |acceleration| as the C2 whisker first crossed a ridge, compared to when it first crossed an equivalent cylinder position on the Smooth stimulus ("fictive ridge"). On ridges, C2 whisker acceleration increased significantly relative to pre-ridge baseline, and was greater than acceleration on fictive ridges (Figure 3D, STAR Methods). The slight increase in acceleration during fictive ridge crossing reflects a bias in selecting first ridge crossings, which are constrained to be moments of forward whisker movement. Randomly sampled whisker traces from Smooth trials, which include both forward and backward whisker movement, showed no bias (Figure S3C). Thus, ridges cause an increase in the local number and magnitude of stick-slip events compared with smooth surfaces.

S1 coding of whisker touch and surface roughness

To determine how whisker touch, roughness, and local ridge geometry are encoded in S1, we made extracellular single-unit recordings using multi-site linear probes while mice performed the Rough-Smooth discrimination task. Recordings were made in C1 or C2 whisker columns, targeted by intrinsic signal optical imaging and confirmed by histological

recovery of fluorescent tracer relative to cytochrome oxidase-stained barrels (Figure 4A). We isolated single units by spike-sorting from 4 adjacent channels treated as one tetrode (Figure 4B). Overall, 170 C1 column units and 256 C2 column units were recorded in 15 penetrations in 5 mice spanning L2/3 to L6. We distinguished fast spiking (FS) from regular spiking (RS) units based on trough-to-peak width of the average spike waveform (Figure 4C). We determined unit depth relative to the L4-L5A border, identified by current source density analysis of local field potentials that were recorded simultaneously with spikes (Figure 4D, Figure S4, STAR Methods). Firing rates were low and skewed in L2/3, L4 and L6, and higher in L5 (Figure 4D). Median firing rates per layer were (in Hz), L2/3: 0.45 ± 0.14; L4: 1.12 ± 0.22; L5A: 3.29 ± 0.82; L5B: 5.10 ± 1.26; L6: 1.24 ± 0.41 (± CI_{95}).

To test whether units responded to whisker-cylinder touch, we compared firing rates in 650 ms windows before and after the static introduction of the stimulus cylinder at trial onset (Figure 5A). Touch onset was defined as occurring 400 ms before the final stimulus cylinder position, corresponding to 2.22 ± 0.05 cm from the mystacial pad. As expected in S1, touch drove firing rate changes in the majority of units (85.9%, 366/426), 89.6% of which were touch-excited and 10.4% of which were touch-inhibited (Figure 5B). Responsive units were distributed evenly across layers and across RS and FS units (Figure 5C). Nearly all L4 and L2/3 units were touch-excited. Touch-inhibited units tended to be RS units located in L5-6 (78.0%, n = 46; Figure 5C).

To test how units encode Rough stimuli, we examined firing rates during smooth->rough transitions (Figure 5D, STAR Methods). Rough surface onset drove firing rate changes in 56.1% (239/426) of units, of which 74.1% were excited and 25.9% were inhibited (Figure 5E). In contrast, smooth->smooth transitions on Smooth trials did not systematically modulate firing rate (Figure S5A), and smooth->smooth and smooth->rough modulations were uncorrelated within units (r^2= 0.01, p=0.02, Figure S5B). Thus, firing rate modulation in Rough trials was texture-related. Roughness responsive units were found in both C1 and C2 columns, though C1 contained a slightly higher proportion of texture inhibited units (Figure S5C). Rough-responsive RS units were most prevalent outside L4 (Figure 5F), while rough-responsive FS units were evenly distributed across layers (p = 0.84, χ^2 = 0.04, d.f. = 1). We compared the mean response to touch vs. the mean response to roughness for each unit (Figure 5G, STAR Methods). While most units that increased firing to touch also increased to roughness, 31.8% of touch-increased units decreased firing to roughness, suggesting a non-monotonic response to increasing tactile intensity.

How well mean S1 firing rate encodes roughness is unclear in behaving rodents (von Heimendahl et al., 2007; Jadhav et al., 2009; Safaai et al., 2013; Zuo et al., 2015). To address this, we compared firing rates on Rough vs. Smooth trials during the palpation window, which ends just prior to behavioral decision. For each unit, firing rate on all trials was z-scored to Smooth trial firing rates (Figure 5H). Average firing was higher on Rough than Smooth trials (p < 0.001; paired t-test, n = 426 units), and lower during epochs of whisking in air (p <0.001; paired t-test). Whisking in Air consisted of Catch trials, which had rapid whisking, but no touch (Figure 2C), and quiescent inter-trial epochs. Thus, roughness elicits both increases and decreases in RS unit firing, with a net significant, but

modest, increase in overall firing rate. In contrast, whisker-cylinder touch drives a more robust and uniform firing rate increase across S1 layers.

S1 coding of local features: slips and ridges

To examine how S1 encodes local surface features, we detected columnar whisker slips and aligned S1 spikes relative to the slip peak (Figure 6A). Firing rate increased with increased slip amplitude in all cortical layers (Figure 6B). Responses were strongest for slips ≥ 2.5 SD (Figure S6A). We identified slip-sensitive (SS) units by comparing spike rate 20 ms before and after slip peaks for slips ≥ 2.5 SD ($\alpha = 0.05$, paired t-test). 43.9% (187/426) of S1 units were SS, with the remainder considered not slip-sensitive (NSS). Slip-evoked spikes were temporally precise (mean 5.6 ± 0.6 ms jitter, 85.5% of slip-excited neurons had < 10 ms jitter (142/166)). Slip-excited units in L4 had the shortest slip response latency (6.4 ± 1 ms), and lowest temporal jitter (4 ± 1 ms, medians ± CI_{95}; Figure S6B–C). C1 slips modestly suppressed spiking to C2 slips in C2 column units, but C2 slips did not suppress spiking in the C1 column (Figure S6D–E), consistent with known direction bias for surround suppression (Jacob et al., 2008; Kida et al., 2005). L4 contained the largest proportion of SS units (55.7%; Figure 6C). SS units were significantly more likely to be FS units (64.9%) than RS units (32.7%; $p < 0.001$, 2-way z-test of proportions; Figure 6C). In addition, SS FS units were almost exclusively slip-excited (96.9%) compared with 79.8% of SS RS units (Figure 6C).

Individual ridges also evoked spiking responses in S1. We measured ridge responsiveness by aligning spikes to time points when whiskers crossed onto or off of bars (ridge-crossing) (Figure 6D). On average, units showed a small increase in firing rate to ridge crossing (Figure 6E). To identify ridge-sensitive (RDS) units, we compared firing rate 20 ms before and after ridge-crossing ($\alpha = 0.05$, paired t-test). Unlike slips, only 11% of units RDS (n = 48 units) with the highest proportion of RDS units in L5B (20%, Figure 6F). Ridges evoked firing rate increases in most RDS L2/3, L4 and L5B units, but decreases in most RDS L5A and L6 units (Figure 6F).

SS and RDS units were highly overlapping with units that responded to touch and roughness (Figure 6G). Considering SS and RDS units in one category (‘local units’), 89.4% of local units were also touch-responsive, and 63.9% of local units were also roughness-responsive. Thus, half of all responsive units (51.7%, n= 208/402) responded to at least one macroscopic and one local feature of touch.

The spatial clustering of slips at ridges (Figure 3) suggests that S1 spikes may also cluster near ridges. To test this, we calculated mean spike count for each C2 column unit as a function of whisker position along the stimulus surface in 0.3mm spatial bins (Figure 6H; STAR Methods). This revealed clear spatial structure in spiking at ridge locations on the 4, 8 and 10 mm gratings, with increased spike counts at ridge onsets. Sandpaper and 2 mm grating stimuli evoked spatially indistinct increases in spike count, similar to slips (Figure 3C). We estimated the spatial precision of ridge-related spiking in C2 units by measuring the location of the first spike peak relative to the first ridge. This revealed a mean spatial error of 0.96 ± 0.66 mm (± SD, Figure 6I). Ridge coding in C1 units was less distinct (data not shown), likely because C1 bent across multiple ridges even at the largest spatial period

(Figure S3B). Thus, S1 units encode local surface features with a resolution of ~1 mm, in addition to encoding macroscopic surface texture.

Contribution of slip-related spikes to the firing rate code for texture

In the slip hypothesis for texture coding, rough surfaces generate increased whisker slips, which evoke higher firing rate in S1 (von Heimendahl et al., 2007; Jadhav et al., 2009). However, whether slips are the major factor driving increased firing rate on rough surfaces is not clear, and trial-to-trial variability in slips and slip-evoked spikes may prevent accurate decoding of rough vs. smooth on single trials. To test these questions, we analyzed spiking in simultaneously recorded unit populations (n = 15, each from 1 session, range 6 – 50 units, mean = 28.4 units, from total of 5 mice). Each population spanned multiple cortical layers in a single C1 or C2 column. An example population of 32 simultaneously recorded units, responding on a Rough trial, is shown in Figure 7A. Across all 15 populations, mean unit firing rate was higher on Rough than Smooth surfaces (Figure 7B). To determine what amount of Rough firing rate was due to slips, we removed all spikes within 0 – 20 ms of each columnar whisker slip (Figure 7C). This abolished the difference in mean unit firing rate between Rough and Smooth surfaces ($p = 0.46$, paired t-test; Figure 7D). However, because slips are more prevalent on Rough trials, this procedure removed a larger proportion of time on Rough (41.8% ± 4.6%) than Smooth (29.4 ± 4.2%) trials (Figure S7A). Thus, elevated mean firing rate on Rough trials could be due either to temporally precise, slip-evoked spikes or to a temporally broader increase in firing rate correlated with roughness.

To address this issue, we tested the effect of regressing out, for each unit, the linearly expected firing rate evoked by each slip in each trial (Figure S7B). We first binned trials based on mean slip rate and amplitude (Figure 7E–F). Figure 7G–H and J–K show mean unit firing rate before (solid lines) and after (dashed lines) regressing out predicted slip-evoked spikes within binned trials. For SS units, firing rate increased with trial-average slip rate, and regressing out slip spikes abolished this relationship (Figure 7G). We found similar effects for firing rate as a function of slip amplitude (Figure 7H). Overall, mean SS firing rate was higher on Rough than Smooth stimuli, and this difference disappeared after regressing out slip spikes ($p= 0.398$, paired t-test, n = 187, Figure 7I).

NSS unit firing rate also differed between Rough and Smooth, but was more weakly related to slip rate, and regressing out slip spikes had only modest effects on slope (Figure 7J). NSS firing rate did increase with slip amplitude, but this was unaffected by regressing out slip spikes (Figure 7K). Overall NSS unit firing rate was higher on Rough than Smooth stimuli, even after regressing out slip-spikes (Figure 7L). Thus, NSS units code a separate (non-slip) feature that differs between Rough and Smooth, and which correlates with slip amplitude.

Altogether, these findings indicate that slips contribute to elevated firing rate on Rough surfaces for SS units, but not NSS units, and that a non-slip signal also exists that drives higher firing rate on Rough surfaces, particularly in NSS units. This non-slip signal may be axial force in the follicle (Bush et al., 2016) related to increased whisker bend with vertical height of the ridges. Indeed, in a small subset of experiments, we performed full whisker imaging at high frame rate and estimated C1 whisker follicle forces during Rough and

Smooth surface contact (STAR Methods). These measurements showed increased axial force when the whisker was on a ridge vs. on the smooth surface (Figure S7E–G).

To test whether SS unit firing rate (which incorporates slip-related spikes) or NSS unit firing rate (which contains the non-slip signal) better encodes Rough vs. Smooth stimuli, we trained a GLM to predict Rough vs. Smooth stimuli from the mean firing rate of each unit for each recording (Figure 7M). We tested performance on hold out trials for either the full model, or with SS or NSS unit coefficients zeroed (equal number of NSS and SS zeroed, n = 13 sessions in 5 mice, STAR Methods). The full model correctly discriminated 85.5 ± 5.6% of Rough vs. Smooth hold-out trials (Figure 7N), similar to mouse behavioral performance and to the performance of our slip decoder (Figure 2D). The model weighted RS units higher than FS units (Figure S7H). Removing SS units from the Rough vs. Smooth model significantly decreased correct texture discrimination to 59.9 ± 7.7% accuracy, and this decrease was greater than removing an identical number of NSS units (72.8 ± 5.2% accuracy, p= 0.020, paired t-test, Figure 7N). Thus, while both SS and NSS units show texture-related firing rate differences, SS units carry more Rough vs. Smooth information on single trials.

To determine whether S1 unit firing rate also accurately predicts animal behavior (Hit, Miss, FA, CR), we built a multinomial decoder to predict mouse behavioral choice from single-trial spike rate using all units from sessions with good behavior (STAR Methods, Figure S8). The model successfully predicted behavioral choice above chance (25%) on single trials (Figure S8A). Mistakes made by the model were also informative. Hit trials were frequently confused with Miss trials (Figure S8B–C) and FA with CR trials (Figure S8D–E). More weakly, on trials with implied stimulus type prediction error, the decoder showed a trend toward choosing the correct Lick/No Lick behavioral outcome (i.e. predicting CR on Miss trials, Figure S8C). Overall, the spiking-based decoder predicted more licks on Hit than Miss trials, and on FA than CR trials (Figure S8F), similar to the whisker slip-based decoder (Figure 2E). Thus, while the dominant variable coded in S1 is stimulus type, S1 spike trains additionally predict behavioral choice.

S1 firing discriminates between rough surfaces

S1 often represents precise features of tactile stimuli even when that information is not used for behavioral performance (de Lafuente and Romo, 2005; McGuire et al., 2016). We therefore tested whether S1 neurons discriminate between individual Rough surfaces, even though mice were not trained to do so. Texture selectivity was defined as a significant difference in mean firing rate within the palpation window across Rough stimuli ($\alpha = 0.05$, one-way ANOVA). 18.3% of units (78/426) were texture-selective (TS). Six examples are shown in Figure 8A–B. 49% (38/78 units) responded maximally to one or more of the 4 grating stimuli, and 37% (29/78 units) responded maximally to the Coarse sandpaper (Figure 8C). Most TS units responded weakly to Smooth and Air, except for a small fraction (11/78) that were also selective among grating frequencies (Figure 8C, U4 in Figure 8B). TS units were distributed across cortical layers similarly to roughness-responsive units (Figure 5F), with most TS units occurring in subgranular layers (60.3%, 47/78). The large majority of TS units were RS units (78.2%, 61/78, Figure 8D).

To test whether the identity of specific stimuli could be decoded from firing rate of the S1 unit population, we trained a multinomial GLM to predict stimulus identity from unit firing rate (STAR Methods). Because TS units were rare, no single recording session captured the full diversity of spatial period tuning. Therefore, we combined all units into one pseudo-population (n=396 units, 4 mice) and generated 200 trials of data by bootstrapping from measured spike trains for Air, Smooth, 2–10 mm gratings, and P150 sandpaper stimuli (7 stimuli, ~28 trials/stimulus). The model was tested on held-out data, and decoded stimulus identity well above chance (chance = 14.3% (1/7), Figure 8E). The model performed best at classifying Air (100% correct), Smooth, (97.6% correct), and the Coarse sandpaper (71.3% correct), but also distinguished individual grating stimuli well above chance (55.5 ± 9% mean accuracy across the 4 gratings). Fitting a similar multinomial model using C1 and C2 whisker slip rate and amplitude as predictors classified Air (82.5%), Smooth (39%) and Coarse (52%) trials, but failed to distinguish between gratings above chance (p=0.054, one-tailed t-test, 16.9 ± 2.7% mean accuracy across 4 gratings, Figure 8E). This suggests that neural responses encode precise spatial or temporal whisker patterns related to the different tactile gratings which are not present in the mean slip properties on each trial.

To probe how specialized tuning in TS units arises, we first compared the proportion of TS and not texture-selective (NTS) units that responded to columnar whisker (CW) vs. surround whisker (SW) slips. 59.0 % of TS units (46/78) were also SS. The same proportion of TS and NTS units responded to CW slips, but a higher proportion of TS units responded to SW slips (Figure 8G–H), suggesting broader spatial response in TS units. Analysis of mean slip-triggered PSTHs of TS and NTS units (Figure 8I–J), showed that TS units had temporally broader responses to slips than NTS units (Figure 8K). Thus, TS units appeared to have broader spatiotemporal response properties, which may allow selectivity among Rough stimuli to be synthesized from multi-whisker spatiotemporal cues.

Discussion

Slips as elementary events in tactile sensation

In active tactile sensation, moving sensors interact frictionally with object surfaces to generate irregular, stick-and-slip motions that are a major component of the sensory signal (Schwarz, 2016). This may also be true for fingertips, where lateral forces create stick-slip skin micromotions and are especially sensitive in activating primary afferents (Delhaye et al., 2014; Johansson and Westling, 1987; Weber et al., 2013). Whisker slips were previously studied as a cue for surface roughness, using macroscopically homogeneous surfaces like sandpapers. Natural whisking produces spatially probabilistic slips on these surfaces, and average slip rate and amplitude correlate with roughness (Jadhav and Feldman, 2010; Jadhav et al., 2009; Wolfe et al., 2008). But natural surfaces also include spatially localized geometric features, in addition to macroscopic roughness. How these two spatial scales are simultaneously encoded is not known. Our results indicate that as whiskers explore ridged surfaces, slip-evoked spikes generate an instantaneous code for spatially localized ridges, and contribute to a slower, time-averaged code for macroscopic roughness, thus contributing to both scales of information.

We used a closed-loop behavioral paradigm with active whisking and virtual locomotion past surfaces. Locomotion is an attentive, information gathering state that enhances cortical sensory responses (Niell and Stryker, 2010). Whiskers are essential for wall-guided locomotion like the stimulus cylinder used here (Sofroniew et al., 2014). We found that mice readily discriminate rough from smooth texture patches during locomotion, as they do for statically presented textures (Chen et al., 2013, 2015). This task design promoted rich trial-to-trial variability in whisker-surface trajectories, which allowed us to identify whisker motion features and S1 spiking associated with ridges and textures at varying positions within the whisking field.

Coding of slips and texture

Higher friction on rough surfaces increases the average rate and amplitude of slips (Arabzadeh et al., 2005; Jadhav et al., 2009; Ritt et al., 2008; Wolfe et al., 2008). In the slip hypothesis for texture coding, these additional slip-evoked spikes increase average firing rate in S1, providing the primary neural code for roughness (Jadhav and Feldman, 2010). However, whether slips adequately explain single-trial roughness discrimination has been unclear (Chen et al., 2015; Jadhav et al., 2009). We compared slip sensory data, mean firing rate for S1 units, and behavioral performance in mice actively engaged in a roughness discrimination task. Slips predicted rough vs. smooth stimuli as accurately as mice did behaviorally, and mouse errors correlated with trial-by-trial variation in slip data (Figure 2D–E). This shows for the first time that whisker slips are sufficient to explain behavioral discrimination of rough and smooth stimuli on individual trials.

Slips evoked time-locked spikes in 40% of touch-responsive units in S1, and slips were responsible for increasing mean S1 firing rate on rough vs. smooth surfaces in SS units (Figure 7I). NSS units also fired more on Rough surfaces, but this was due to a separate, non-slip texture-related signal, possibly reflecting increased whisker bend and axial force in the follicle (Figure S7E–G). Together, these signals generated a robust firing rate code for texture, and we could decode Rough vs. Smooth stimuli from single-trial firing rate of S1 units as accurately as mouse behavior (Figure 7N). Removing SS units from the decoder preferentially impaired decodability compared to removing NSS units (Figure 7N). Thus, slips and slip-evoked spikes contribute to a firing rate code in SS units that is critical for coding surface roughness.

Coding of local shape

How the tactile system encodes spatially precise geometric features of surfaces during active touch is unknown. In primate S1, many neurons spike to the edges of raised letters scanned across a passive, non-moving fingertip (Phillips et al., 1988). This implies both an instantaneous code for local features in each cell’s receptive field, and an isomorphic representation of spatial features across cortical space. How fine spatial features are encoded during active touch in a moving fingertip is entirely unknown, largely because the skin-surface interface is hidden and complex skin distortion alters receptive fields (Johansson and Flanagan, 2009). In contrast, individual whiskers can be precisely tracked during contact on fine surface features. We found that slips and S1 spikes accumulate at grating ridges (Figure 3, Figure 6H). This occurred despite the complexity of whisker trajectories on the surface,

and indicates that individual slips provide an instantaneous, spatially and temporally local code for geometrically precise surface features (Schwarz, 2016). This is the first observation, to our knowledge, of a spatially precise code for local surface features during active tactile sensation.

This instantaneous code may be used to construct an explicit spatial representation of the location of surface features. This would require reading out instantaneous spikes in reference to a whisker position signal, for example the whisking phase signal present in S1 from whisker reafference (Curtis and Kleinfeld, 2009; Severson et al., 2017; Wallach et al., 2016) and the whisking set point and amplitude signals present in M1 (Kleinfeld and Deschênes, 2011). For C2 unit spikes, the resulting spatial representation could achieve ~1 mm resolution (Figure 6I), assuming the whisker position signal has similar error to our whisker tracking error (~1 mm, Figure S1E). True spatial precision could be even better, given that our spatial estimates are limited by this tracking error. S1 coded the presence of each ridge despite the fact that mice were not required to discriminate ridge position or spatial frequency. Prior studies also found precise temporal coding in S1, even when that information was not used for behavioral decision (Hernández et al., 2000; McGuire et al., 2016).

Whether mice actually use precise S1 spike timing for spatial perception is unclear. Rats show some limited ability to distinguish different virtual spatial frequencies of S1 microstimulation, suggesting that spike timing is perceptually relevant (Georgieva et al., 2014). During full-field exploratory whisking, object location is represented by interaction of precisely timed contact signals and whisker position signals (Kleinfeld and Deschênes, 2011). But in other behavioral conditions, mice adopt a directed search strategy that localizes objects based on spike rate, not precise timing (Hires et al., 2013b; O'Connor et al., 2010b, 2013). Additional multi-whisker cues may provide more accurate spatial perception in fully whiskered animals (Ahissar and Arieli, 2001; Anjum et al., 2006), but may still depend on precise timing.

Multiplexed coding of local shape and texture

Our results indicate that slip-related spikes form a dual, multiplexed code for both precise local features and macroscopic roughness. Multiplexed temporal and rate codes are evident in primate S1 during vibrotactile discrimination (Harvey et al., 2013; Luna et al., 2005; Mountcastle et al., 1969) and in hippocampus for coding current location vs. planned or remembered sequences (Foster and Knierim, 2012). We found that 90% of units responding with time-locked spikes to local features also encoded macroscopic tactile features (touch and roughness) by changes in mean firing rate over hundreds of ms (Figure 6G). Whether animals have simultaneous access to local shape and texture is not known, however information provided by units multiplexing these features may explain why rate and timing carry independent information about texture in rat S1 (Zuo et al., 2015).

While many units showed an intensity-like code with monotonically increasing firing rate to increasing spatial frequency, a significant proportion of TS units had non-monotonic tuning curves (Figure 8B–C). This is consistent with the roughness tuning curves observed in Ca^{2+} imaging in L2/3 neurons, where the mechanism for how non-monotonic roughness tuning

arises is unknown (Garion et al., 2014). The majority of TS units were SS (60%) and therefore carried both local and macroscopic codes. Interestingly, TS SS units exhibited broader spatiotemporal responses to slips than NTS SS units (Figure 8G–K). Thus, multi-whisker temporal patterns of local input might be important for generating spatial period tuning in TS units.

While local and macroscopic codes intermix within single neurons, layer-specific differences in the multiplexed code are evident. L4 neurons code whisker contact with low firing rates (Figure 4D), high temporal precision, and minimal noise (Hires et al., 2015). L5 units have high firing rates (Figure 4D) and broad receptive fields (Chapin, 1986; Manns et al., 2004). We observed that L4 had the highest proportion of slip-responsive units (Figure 6C) and lowest response latency and jitter (Figure S6B–C), as observed previously (Jadhav et al., 2009). L5 had fewer slip-responsive units and a higher proportion of roughness responsive and spatial frequency selective units (Figures 5F, 8D). This suggests that the multiplexed code in L4, which contains prominent short time-scale information about contact and slips, is transformed outside of L4 into a more rate-dominant code for macroscopic features including tactile shape.

STAR Methods

CONTACT FOR REAGENT AND RESOURCE SHARING

Further information and requests for resources and reagents should be directed to and will be fulfilled by the Lead Contact, Dan Feldman (dfeldman@berkeley.edu).

EXPERIMENTAL MODEL AND SUBJECT DETAILS

Adult male mice (C57BL/6, Harlan) had head-plates implanted at P89 ± 44 days and neural data were recorded at P265 ± 125 days (n=5, mean ± SD). All procedures were performed in accordance with UC Berkeley Animal Care and Use Committee and meet NIH guidelines. Mice were housed singly or in pairs with reverse light-dark cycle (12 hr each phase). Behavior experiments were conducted at the same time of day during the dark (active) cycle, 5 days a week. Home cages included an enclosure and running wheel (Fast-Trac #K3251 and Mouse Igloo #K3327, Bio-Serv).

METHOD DETAILS

Surgical procedures

Head-plate implant: Mice were anesthetized using 2% isoflurane (vol/vol) and placed in a stereotaxic apparatus. Body temperature was maintained at 37 °C using a feedback-controlled heating pad (FHC, 40- 90-8D) and a small incision was made in the scalp. The skull was cleaned and a stainless steel head plate was implanted using dental cement (Metabond, Parkell), aligned to bregma and midline (Figure S1A). Mice recovered for at least 1 week before start of behavioral training. After training, a cranial chamber was drilled into the cement, centered on C1 and C2 whisker columns in S1. Intrinsic signal optical imaging (ISOI) was performed through the intact skull, as in Drew & Feldman, 2008, to localized C1 and C2 functional columns This procedure was performed under Isoflurane (1.5%) + chlorprothixene (0.025 mg/kg) anesthesia. Afterwards the cranial chamber was

filled with silicone elastomer (Kwik-Cast, WPI), and sealed with a thin layer of dental cement.

In vivo electrophysiology: Mice were briefly anesthetized with 2% isoflurane. A small craniotomy (~ 0.1mm) was made over the C1 or C2 column and mice were transferred to the behavior rig. Recording locations were measured relative to vascular landmarks for later reconstruction. A linear silicon probe (A1x16-5mm-25-177-A16 or A1x32-5mm-25-177-A32, Neuronexus) was slowly inserted to desired depth (500–900μm; Sutter MP285). The chamber was then resealed with silicone elastomer and the probe was allowed to settle (45 minutes). After recording, the probe was removed and the chamber was sealed with a thin layer of dental cement.

Smooth vs. Rough discrimination training—Mice were water restricted to 85% ad lib weight and handled for 5–10 minutes for 2 days before training. Animals were acclimated to head-fixation (1–2 days) and taught to lick for water rewards (1–2 days; 2–5μl rewards paired with a 30ms 2.8kHz tone). Lick responses were scored and rewarded when Instantaneous lick rate stayed below 1Hz for at least 1 second and subsequently exceeded ~3Hz (Figure 1C). Rewards were then paired with rough stimuli (1–2 day). Early training used 50:50 Rough:Smooth trials in block delivery (5±1 trials) with open-loop (fixed velocity) stimulus presentation. Early training ended when mice performed with 5–10 correct transitions from Go to No-go blocks paired with overall session accuracy > 70% for two consecutive days. Rough and Smooth stimuli were then presented randomly (open-loop) until criterion (2 consecutive days of > 75% performance). Animals then transitioned from open-loop presentation to closed-loop presentation (1–4 days). Upon stable performance, rows of right-side whiskers were gradually trimmed over 5 days until all but C1–C2 remained. If performance decreased, whisker trimming was paused until behavior recovered. Trials started when mice withheld licking for 2–3 seconds. The response window (1–2 seconds) started with stimulus movement (open-loop) or by self-initiation by running 1–2cm (closed-loop). Hit triggered 3μL water reward paired with a 30ms 2.8kHz tone. False Alarms triggered a 300ms 10kHz tone and a 5 second time out, while no action was taken for Correct Rejections or Misses. Catch trials (7% of trials; 50:50 Go:No-go) were identical to stimulus trials except the stimulus cylinder did not contact the whiskers. Catch trials were used to measure active whisking in Air and to test for the use of non-tactile cues. All training was performed in total visual darkness (850nm IR illumination) accompanied by loud white noise. Task structure was controlled by an Arduino (Leonardo) in communication with MATLAB, using custom software.

Stimulus cylinder—Rough stimuli consisted of gratings with 2, 4, 8, and 10mm spatial period and one section of coarse P150 sandpaper whose height above the cylinder surface was matched to the gratings (0.8mm above surface). Gratings had 50% duty cycle (e.g., 2mm grating consisted of 1mm bars and 1mm gaps). Gratings were constructed from ±0.05 mm precision strips of 0.03” shim plastic (P/N: 9513K75, McMaster-Carr) glued (ZAP, PAAPT02) in 30mm patches to an acetate plastic sheet (3M, PP2950) attached to an acrylic wheel (OD: 12.64cm, TAP Plastics). The smooth area preceding rough patches and the Smooth stimulus surface both consisted of acetate plastic alone. Glue was also applied above

and below Smooth sections to control for the presence of glue odor and all stimuli were wiped cleaned with odorless, water-based detergent (Process NPD, Steris) before every training session.

To present stimuli yoked to the mouse's movement during each trial, the stimulus cylinder was rotated with a stepper motor using 20,000 step/rotation micro-stepping (STM17R, Applied Motion). Between trials, stimuli were randomized using a paradigm that took the same number of steps to reach any position on the stimulus cylinder. In addition, we mounted a sham stepper motor next to the stimulus motor which presented randomly chosen stimuli during each trial. These steps were taken to prevent motor sounds from being used as task cues. Stimulus cylinder motors were controlled by independent Arduino Uno R3's using custom code. Real-time closed-loop stimulus delivery was achieved by switching stepper motor rotation control to pulses generated by the running disk rotary encoder (P/N: H5-1000-IE-S, US Digital). The running disk consisted of a 6″ diameter disk machined from 1/16″ thick acrylic (P/N: 8560K172, McMaster-Carr) with a polypropylene mesh adhered for traction (mesh P/N: 9265T51, McMaster-Carr). A 4:1 run:move ratio was used to allow full running movements with a small stimulus cylinder. Mice traveled ~6 cm to bring the stimulus patch into whisker contact (~1.5 cm of stimulus rotation).

The stimulus cylinder stepper motor was mounted to a linear actuator that retracted the stimulus cylinder between trials, and brought it back into whisker contact prior to the start of each trial. These were P/N LP28 with NEMA11 motor, Parker Automation; Nippon Pulse AD1431 motor driver, 16x μsteps, 3,211 steps/cm. This linear sled was positioned at an angle of 52° from midline, and moved at a velocity of 3.1cm/s. The linear onset had an S-curve velocity profile (max acceleration = 12 cm/s^2 in 150ms onset/offset acceleration trapezoids; example trajectory in Figure 5A). Touch onset occurred during this linear translation of the stimulus assembly to the mystacial pad. During stimulus delivery (full whisker contact), the stimulus cylinder was 1.45 ± 0.05cm from the mystacial pad. During stimulus randomization, the stimulus assembly was retracted to 2.94 ± 0.06 cm from the mystacial pad, where there was no whisker contact.

Spike sorting—A 32 channel TDT System 3 (RZ5D) was used to digitize running/motor movement signals (48kHz) and neural signals (24.4 kHz) recorded from 16 channel (A1x16-5mm-25-177-A16) or 32 channel (A1x32-5mm-25-177-A32, Neuronexus) linear probes for post hoc filtering. NeuroNexus A32-Z32 adapter was used and corrected for erroneous hardware mapping (see: Additional Resources). Channels used for spike processing (Bessel filter 300–6,000 Hz; MATLAB filtfilt ()) were further processed by common average referencing (Ludwig et al., 2009). All spike detection, clustering and sorting was performed using UltraMegaSort 2000 (Hill et al., 2011). Linear probe electrode sites were broken into groups of 4-adjacent sites (tetrodes) and spike events were detected 3–4 SD below the mean with a 0.75 ms shadow period. Events were then clustered using k-means clustering (kmeans_clustersize =50), aggregated based on interface energy (agg_cutoff = 0.2; Fee et al., 1996) and manually inspected on the basis of spike waveform, stability in time, and inter-spike interval refractory period violations (< 0.5% of intervals < 1.5ms). Units were classified as fast-spiking if trough to peak duration was below 0.45ms (Barthó et al., 2004).

Current source density for estimation of laminar boundaries—Slip-evoked local field potentials (LFPs; Butterworth filter 0.1–300 Hz; MATLAB) were cleared of electrical artifacts (>15 SD above mean), normalized to account for differences in channel impedance, and interpolated between channels (25um site spacing, 10–20x interpolation) before calculating the second spatial derivative (Freeman and Nicholson, 1975). CSDs were convolved with a 2D Gaussian and the zero-crossing encountered between the most negative current sink (putative L4) and the next current source (putative L5A) was deemed the L4/L5A boundary. This search was restricted to sites estimated to lie 400–650um below pia as measured via micromanipulator. Units were then assigned to layers using layer boundaries as in (Lefort et al., 2009).

Histology—After the final recording in each mouse, 3 fluorescent tracks were created relative to landmarks using a silicone probe covered in 1,1′-Dioctadecyl-3,3,3′,3′-Tetramethylindo-carbocyanine Perchlorate (DiI, D282, ThermoFisher). Mice were deeply anesthetized with isoflurane and euthanized. The brain was removed and fixed in 4% paraformaldehyde. The cortex was flattened, tangentially sectioned (50μm) and stained for cytochrome oxidase (CO) to identify whisker barrels in L4. Fluorescent tracks were imaged relative to barrel boundaries to reconstruct experimental penetration locations.

Behavioral data analysis—Mice typically exhibited all-lick behavior for the first few trials each day (likely due to initial thirst), then stable behavioral performance for most of the day, followed by no-lick behavior at the end of the day (likely due to satiety). We quantified daily discrimination excluding these early and late epochs. To do this, we identified the first and last trials that exceeded $d' = 1$, calculated in a sliding window of 50 trials centered on the current trial (Siegle et al., 2014):

$$d' = z(hit) - z(fa),$$

where *hit* = hit rate, *fa* = false alarm rate, and z= inverse of the normal cumulative distribution function, with mean = 0 and standard deviation = 1. We implemented the log-linear correction for rate values of 0 and 1 (Stanislaw and Todorov, 1999). All discrimination metrics (percent lick, d′, % correct) were calculated using all trials between the first trial with a sliding $d' > 1$ to the last trial with a sliding $d' > 1$. This criterion excluded trials dominated by satiety effects at the beginning and ending of a training session, while retaining the vast majority of trials (85% = 66,906/78,713 trials). Trials were also excluded if the mouse failed to run far enough trigger the response window.

Whisker data analysis—Whisker data were analyzed from all trials i) that the mouse successfully initiated, ii) in which the mouse ran far enough to touch the stimulus patch and trigger response window onset, and iii) in which whiskers were not obscured during imaging.

Identifying whisker position, slips: Whiskers were imaged as 1D shadows in a collimated IR laser curtain (904nm laser, P/N: L904P010, Thorlabs) at 4kHz using a custom linear CCD array 0.8–1cm from mystacial pad (Figure S1C). Methods were as in Jadhav et al.,

2009. Pixel positions were spatially corrected for lens distortion. Raw movies were pre-processed by subtracting median pixel values. Whisker shadows were detected and the peak localized by Gaussian fit, which interpolates between pixels. Whisker position traces over time were de-noised by down-sampling to 1kHz (decimate( ), MATLAB) and up-sampling with a spline fit to the original sampling rate. Whisker shadows were localized within a 2D plane in coordinates from mouse bregma using a calibrated webcam (C510, Logitech; MATLAB 2014b, Machine Vision Toolbox). C1 and C2 whisker follicle locations were also known in stereotaxic coordinates relative to bregma (Figure S1B), both for resting whisker position and for active set position (~1mm rostral of resting position, measured via high-speed imaging). This allowed whisker position to be calculated in angular coordinates from the follicle and in absolute positions in space (mm along stimulus cylinder). Position estimates of whisker contact on surfaces were corrected for bend by fitting a Gaussian model to projection errors measured in high-speed video analysis (Figure S1). Acceleration was calculated numerically as the second derivative of position with respect to time (diff( ), MATLAB). Slips were detected as peaks in acceleration that exceeded ± 2.5 SD from the mean acceleration within each session (for each whisker), unless otherwise indicated.

Whisker kinematics: Whisker imaging was used to identify a palpation window from 50ms before first contact with the stimulus patch in each trial, to 200ms before first lick. A 650ms window was used on no-lick trials. Mean slip rate, amplitude, whisker speed, and rodent speed were calculated in this window for each trial. Slip density was calculated by summing the number of slips per mm along the stimulus during each trial. Ridge-triggered acceleration was calculated by z-scoring |acceleration| during the first two ridge crossings of each grating trial relative to a 30 ms baseline period before ridge crossing (−40 to −10 ms). We tested for differences in these means using a multi-sample ANOVA with repeated measures with Rough and Smooth as factors analyzed across time points ± 15ms from ridge crossing (n = 28 sessions in 6 mice, one session was excluded from this analysis due to insufficient C2 trace sampling of first ridge).

Follicle force estimates using Elastica2D: We performed full whisker imaging during rough-smooth discrimination in 2 additional mice. We imaged whiskers at 220 fps (AVT Prosilica Gige GC660) and fit biophysical models using a manual fitting procedure based on Elastica2D (Quist and Hartmann, 2012). Briefly, we measured whisker shape at rest and mean whisker follicle position during palpation in frames of spatially calibrated video (MATLAB 2014b, Machine Vision Toolbox). Biophysical models used a Young's Modulus of 3–5 GPa at the base tapering to 0.1 GPa at the tip. We designed a graphical user interface to manually set the unobstructed whisker angle and point of contact in a subset of frames. Angle and point of contact were adjusted to align the predicted whisker curvature with the observed whisker curvature. Negative axial force output from Elastica2D was made positive for presentation in Figure S7. A permutation test was performed on mean paired rough vs. smooth axial force difference (n= 2 mice).

Neural Data Analysis—Neural data were analyzed in 5 mice (15 recording sessions) with successful recordings, in the same trials as whisker data analysis. We calculated z-scored responses as:

$$z=\frac{x_{resp}-x_{base}}{\sigma_{base}},$$

where x = mean firing rate and σ = standard deviation across events (i.e. trials or kinematics) during response (resp) or baseline (base) periods. For z-scored PSTHs (zPSTH), time-series data were first averaged within the baseline period, and then x_{base} and σ_{base} were calculated as described above. These scalar values were used to z-score the x_{resp} PSTH time-series from each event, paired t-test statistics were used to determine responsiveness relative to baseline, and the sign of the z-score was used to determine if responsive units increased or decreased firing to a stimulus. The log-modulus transformation (Figure 5G, Figure S5B) was implemented as:

$$\text{logmod}=sign\ (\Delta x)*\log\ (|\Delta x|+1)\,,$$

where $\Delta x = x_{resp} - x_{base}$.

We identified touch and roughness responsive units by performing a paired t-test on mean firing rate in 650ms windows before and after First Contact of roughness onset (Figure 5). Roughness onset was always defined by first C2 contact (Figure 5D), even when recording was targeted to C1 column. This allowed us to analyze roughness responses at the earliest possible onset, which includes responses driven by surround whiskers. ZPSTHs from units classified as increasing, decreasing, or non-responsive were smoothed (MATLAB, 'lowess', 25ms) before calculating the mean and CI_{95} of all units.

We measured slip responses using columnar whisker slips (C1 slips for units recorded in C1 column, C2 slips for units recorded in C2 column), ranging from 1 to 8 SD above baseline (Figure 6B). We found that slips ≥ 2.5 SD above baseline drove consistent responses in S1 (Figure S5A). We identified slip responsive units by performing a paired t-test on mean firing rate 20ms after the peak acceleration of slips ≥ 2.5 SD compared to a 20ms baseline 40ms before the slip peak (Figure 6C). Ridge responses were measured in an identical way using ridge crossing events in the columnar whisker (Figure 6F). Slip response latency was measured using a binless Poisson method (Chase and Young, 2007), with median bootstrapped 95% confidence intervals. Spike jitter was measured in slip-responsive units as the full-width at half-max in the slip PSTH.

We used slip PSTHs to model the change in firing rate expected due to slips, i.e. the change in firing rate linearly predicted by one average slip > 2.5SD in amplitude. This was calculated on each trial for each unit (Figure S7B–D) in order to regress out the effect of slips on rough and smooth trials.

We identified texture selective units by calculating a one-way ANOVA on mean firing rates within the palpation window for each rough stimulus type (10, 8, 4, 2mm and Coarse). Tuning curves represent mean palpation window firing rate to each stimulus.

We calculated the spatial density of spikes near ridges in 0.3mm bins of C2 whisker movement for C2 column units (Figure 6H). For each bin, we calculated the fraction of additional spikes evoked by rough over smooth stimuli as $(SC_{rough} - SC_{smooth})/max\ (SC_{all})$, where SC_{all} was the maximum response of each unit, and SC = mean spike count/mm whisker travel. Note: C1 whisker bend often crossed multiple features (Figure S3B), preventing accurate spatial binning. Therefore only C2 units were included for this analysis.

General linear models (GLMs)—Single trials were decoded using glmnet( ) in MATLAB (Qian et al., 2013) by fitting a multinomial GLM (glmnet( ), 'multinomial') and classifying hold-out data (glmnetPredict( ), 'class') using 10 fold cross-validation (CV). Multinomial coefficient values were corrected for binomial interpretation (Figure S7H). The alpha parameter was left at default value of 1 (LASSO regression), and lambda ('lambda_1se') was calculated within each fold using CV (cvglmnet(), 10 folds). All classification accuracies represent mean model performance on hold-out data across 25–50 iterations of randomly assigned folds. To eliminate bias, training and testing data were randomly re-sampled to have identical numbers of trials within each response category. For whisker decoding of Rough vs. Smooth (Figure 2D), mean C1 and C2 slip rate and |slip amplitude| were used as predictors on each trial within behavioral sessions. An identical method was used to predict lick vs. no lick trials (Figure 2E). Neural decoding of Rough vs. Smooth trials (Figure 7N, Full) used mean firing rate of each simultaneously measured unit on each trial within behavioral sessions. In Figure 7N, the fit neural decoding models then had slip-sensitive (SS) or slip-insensitive (NSS) unit coefficients zeroed in days where the number of NSS could be matched to the number of SS (n=13 sessions in 5 mice). Coefficients for all SS (or random subset of equal number NSS) were set to zero in each session (100 iterations of NSS procedure) and Rough vs. Smooth prediction accuracy was measured.

For discriminating between all stimuli (Air, Smooth, 10, 8, 4, 2mm, and Coarse, Figure 8E), a pseudo-population was created by combining all units and bootstrapping 200 trials of palpation window firing rate responses and fit using 4-fold CV. One recording did not contain all stimulus categories and was excluded from this analysis (n=396 units, 4 mice). To discriminate between all stimuli using whisker kinematics (Figure 8F), mean C1 and C2 slip rate and |slip amplitude| were used as predictors on each trial to predict stimulus category from the same days as neural decoding. Unlike neurons, whiskers were not pooled across days. To predict mouse behavioral choice, Hit, Miss, FA and CR outcomes were predicted from unit firing as described above for each session (10-fold CV, 25 iterations). To ensure the behavioral accuracy of data used for this analysis, only sessions with mean $d' > 1$ were included (n= 12 sessions in 4 mice). Predicted outcomes were re-coded as Lick or No-Lick outcomes for Figure S8F.

Data inclusion, exclusion and replication

Inclusion and exclusion criteria for subjects and data: Criteria for data inclusion and exclusion are discussed in the Results and in other sections of STAR Methods, and are restated here. All mice that learned the task and had successful whisker imaging data (n=7 mice) and/or neurophysiology (n=5/7 mice) were included for analysis (Figure S2A). The

criterion for learning the task was 2 consecutive days of > 75% performance. Trial inclusion criteria are explained above in 'Behavioral Data Analysis'. We obtained 16 sessions of neurophysiological recording data, across 5 mice. Of these, 1 was excluded from the study due to a misalignment in whisker imaging. The remaining 15 sessions were used for all analyses. For the analysis in Figure 8E, which requires that all stimulus types be present, 1 session was excluded because the P150 sandpaper was not presented. For the decoding model of Figure S8, whose goal was to predict animal behavior from neural spiking data, we excluded 1 mouse because its discrimination behavior did not exceed a d' of 1 during the neurophysiology recording sessions, as explained above in 'General Linear Models (GLMs)'.

Sample-size estimation: We did not perform *a priori* sample-size estimation. Instead, our planned goal from the outset was to record from many hundreds of neurons in ≥ 5 mice, as is standard practice in population coding studies. Analysis and statistics were performed on the full dataset, after all data were collected.

Replication, blinding, randomization: Mice were from 5 different litters, tested with identical stimuli and behavioral and recording methods, thus constituting independent replicates. Stimulus order was randomized. For model-based analyses, replication was also implemented at the level of k-fold cross-validation. Experimenters were not blind for data collection or analysis.

QUANTIFICATION AND STATISTICAL ANALYSIS

All statistics were calculated using MATLAB 2012b and custom software as required. Values in the text and error bars in figures are 95% confidence interval of the mean (CI_{95}) unless otherwise stated. Median CI_{95} were determined by bootstrap. Neural data are reported from 426 units recorded in 5 mice across 15 behavior sessions. Additional whisker imaging (without neural measurements) was collected in these 5 mice as well as 2 additional mice for a total of 29 sessions in 7 mice. ANOVA used in time series comparisons were multi-sample repeated measures ANOVA using anova_rm() (MATLAB File Exchange), with p-value reported for group x time interaction, unless otherwise stated. Linear fits and weighted linear fits (Figure 7G–H, J–K) were calculated using LinearModel.fit (MATLAB 2012b).

DATA AND SOFTWARE AVAILABILITY

Custom MATLAB code used for analyses and data will be made available upon reasonable request.

ADDITIONAL RESOURCES

Detailed information on constructing the lickometer, fluid delivery system, and running wheel used in these experiments, as well as instructions for correcting the NeuroNexus A32-Z32 adapter mapping error, can be found online at http://brianisett.com/category/neuroscience/.

Supplementary Material

Refer to Web version on PubMed Central for supplementary material.

Acknowledgments

We thank Janice Chua, Suchetana Dutta, and Karan Patel for animal training and histology; Keven Laboy for analysis discussions. This work was supported by NIH 1R01NS072416 and R37NS092367. B.R.I. was supported by National Science Foundation predoctoral fellowship DGE 1106400.

References

Ahissar E, Arieli A. Figuring Space by Time. Neuron. 2001; 32:185–201. [PubMed: 11683990]

Anjum F, Turni H, Mulder PGH, van der Burg J, Brecht M. Tactile guidance of prey capture in Etruscan shrews. Proc Natl Acad Sci U S A. 2006; 103:16544–16549. [PubMed: 17060642]

Arabzadeh E, Zorzin E, Diamond ME. Neuronal encoding of texture in the whisker sensory pathway. PLoS Biol. 2005; 3:e17. [PubMed: 15660157]

Barthó P, Hirase H, Monconduit L, Zugaro M, Harris KD, Buzsáki G. Characterization of neocortical principal cells and interneurons by network interactions and extracellular features. J Neurophysiol. 2004; 92:600–608. [PubMed: 15056678]

Boubenec Y, Claverie LN, Shulz DE, Debrégeas G. An Amplitude Modulation/Demodulation Scheme for Whisker-Based Texture Perception. J Neurosci. 2014; 34:10832–10843. [PubMed: 25122886]

Brecht M, Preilowski B, Merzenich MM. Functional architecture of the mystacial vibrissae. Behav Brain Res. 1997; 84:81–97. [PubMed: 9079775]

Bush NE, Schroeder CL, Hobbs JA, Yang AE, Huet LA, Solla SA, Hartmann MJ. Decoupling kinematics and mechanics reveals coding properties of trigeminal ganglion neurons in the rat vibrissal system. Elife. 2016; 5:1–23.

Carvell GE, Simons DJ. Biometric analyses of vibrissal tactile discrimination in the rat. J Neurosci. 1990; 10:2638–2648. [PubMed: 2388081]

Chapin JK. Laminar differences in sizes, shapes, and response profiles of cutaneous receptive fields in the rat SI cortex. Exp Brain Res. 1986; 62:549–559. [PubMed: 3720884]

Chase SM, Young ED. First-spike latency information in single neurons increases when referenced to population onset. Proc Natl Acad Sci U S A. 2007; 104:5175–5180. [PubMed: 17360369]

Chen JL, Carta S, Soldado-Magraner J, Schneider BL, Helmchen F. Behaviour-dependent recruitment of long-range projection neurons in somatosensory cortex. Nature. 2013; 499:336–340. [PubMed: 23792559]

Chen JL, Margolis DJ, Stankov A, Sumanovski LT, Schneider BL, Helmchen F. Pathway-specific reorganization of projection neurons in somatosensory cortex during learning. Nat Neurosci. 2015; 18:1101–1108. [PubMed: 26098757]

Curtis JC, Kleinfeld D. Phase-to-rate transformations encode touch in cortical neurons of a scanning sensorimotor system. Nat Neurosci. 2009; 12:492–501. [PubMed: 19270688]

Delhaye BP, Lefèvre P, Thonnard JL, Lefevre P. Dynamics of fingertip contact during the onset of tangential slip. J R Soc Interface. 2014; 11:20140698–20140698. [PubMed: 25253033]

Diamond ME. Texture sensation through the fingertips and the whiskers. Curr Opin Neurobiol. 2010; 20:319–327. [PubMed: 20403683]

Diamond ME, Von Heimendahl M, Arabzadeh E. Whisker-mediated texture discrimination. PLoS Biol. 2008; 6:1627–1630.

Drew PJ, Feldman DE. Intrinsic Signal Imaging of Deprivation- Induced Contraction of Whisker Representations in Rat Somatosensory Cortex. Cereb Cortex. 2008

Ewert TAS, Möller J, Engel AK, Vahle-Hinz C. Wideband phase locking to modulated whisker vibration point to a temporal code for texture in the rat's barrel cortex. Exp Brain Res. 2015; 233:2869–2882. [PubMed: 26126800]

Fee MS, Mitra PP, Kleinfeld D. Automatic sorting of multiple unit neuronal signals in the presence of anisotropic and non-Gaussian variability. J Neurosci Methods. 1996; 69:175–188. [PubMed: 8946321]

Foster DJ, Knierim JJ. Sequence learning and the role of the hippocampus in rodent navigation. Curr Opin Neurobiol. 2012; 22:294–300. [PubMed: 22226994]

Freeman, Ja, Nicholson, C. Experimental optimization of current source-density technique for anuran cerebellum. J Neurophysiol. 1975; 38:369–382. [PubMed: 165272]

Garion L, Dubin U, Rubin Y, Khateb M, Schiller Y, Azouz R, Schiller J. Texture coarseness responsive neurons and their mapping in layer 2–3 of the rat barrel cortex in vivo. Elife. 2014; 3:e03405. [PubMed: 25233151]

Georgieva P, Brugger D, Schwarz C. Are spatial frequency cues used for whisker-based active discrimination? Front. Behav Neurosci. 2014; 8:379.

Harvey MA, Saal HP, Dammann JF, Bensmaia SJ. Multiplexing Stimulus Information through Rate and Temporal Codes in Primate Somatosensory Cortex. PLoS Biol. 2013:11.

von Heimendahl M, Itskov PM, Arabzadeh E, Diamond ME. Neuronal activity in rat barrel cortex underlying texture discrimination. PLoS Biol. 2007; 5:e305. [PubMed: 18001152]

Hernández A, Zainos A, Romo R. Neuronal correlates of sensory discrimination in the somatosensory cortex. Proc Natl Acad Sci U S A. 2000; 97:6191–6196. [PubMed: 10811922]

Hill DN, Mehta SB, Kleinfeld D. Quality Metrics to Accompany Spike Sorting of Extracellular Signals. J Neurosci. 2011; 31:8699–8705. [PubMed: 21677152]

Hires SA, Pammer L, Svoboda K, Golomb D. Tapered whiskers are required for active tactile sensation. Elife. 2013a; 2:e01350. [PubMed: 24252879]

Hires SA, Efros AL, Svoboda K. Whisker Dynamics Underlying Tactile Exploration. J Neurosci. 2013b; 33:9576–9591. [PubMed: 23739955]

Hires SA, Gutnisky DA, Yu J, O'Connor DH, Svoboda K. Low-noise encoding of active touch by layer 4 in the somatosensory cortex. Elife. 2015; 4:1–18.

Jacob V, Le Cam J, Ego-Stengel V, Shulz DE. Emergent Properties of Tactile Scenes Selectively Activate Barrel Cortex Neurons. Neuron. 2008; 60:1112–1125. [PubMed: 19109915]

Jadhav SP, Feldman DE. Texture coding in the whisker system. Curr Opin Neurobiol. 2010; 20:313–318. [PubMed: 20299205]

Jadhav SP, Wolfe J, Feldman DE. Sparse temporal coding of elementary tactile features during active whisker sensation. Nat Neurosci. 2009; 12:792–800. [PubMed: 19430473]

Johansson RS, Flanagan JR. Coding and use of tactile signals from the fingertips in object manipulation tasks. Nat Rev Neurosci. 2009; 10:345–359. [PubMed: 19352402]

Johansson RS, Westling G. Signals in tactile afferents from the fingers eliciting adaptive motor responses during precision grip. Exp Brain Res. 1987; 66:141–154. [PubMed: 3582528]

Kida H, Shimegi S, Sato H, Cam J, Le Estebanez L, Jacob V, Shulz DE, Hemelt ME, Kwegyir-afful EE, Bruno RM, et al. Similarity of Direction Tuning Among Responses to Stimulation of Different Whiskers in Neurons of Rat Barrel Cortex. J Neurophysiol. 2005; 94:2004– 2018. [PubMed: 15972836]

Kleinfeld D, Deschênes M. Neuronal basis for object location in the vibrissa scanning sensorimotor system. Neuron. 2011; 72:455–468. [PubMed: 22078505]

de Lafuente V, Romo R. Neuronal correlates of subjective sensory experience. Nat Neurosci. 2005; 8:1698–1703. [PubMed: 16286929]

Lefort S, Tomm C, Floyd SJ, Petersen CCH. The excitatory neuronal network of the C2 barrel column in mouse primary somatosensory cortex. Neuron. 2009; 61:301–316. [PubMed: 19186171]

Ludwig KA, Miriani RM, Langhals NB, Joseph MD, Anderson DJ, Kipke DR. Using a common average reference to improve cortical neuron recordings from microelectrode arrays. J Neurophysiol. 2009; 101:1679–1689. [PubMed: 19109453]

Luna R, Hernández A, Brody CD, Romo R. Neural codes for perceptual discrimination in primary somatosensory cortex. Nat Neurosci. 2005; 8:1210–1219. [PubMed: 16056223]

Manns ID, Sakmann B, Brecht M. Sub- and suprathreshold receptive field properties of pyramidal neurones in layers 5A and 5B of rat somatosensory barrel cortex. J Physiol. 2004; 556:601–622. [PubMed: 14724202]

McGuire LM, Telian G, Laboy-Juárez KJ, Miyashita T, Lee DJ, Smith KA, Feldman DE. Short Time-Scale Sensory Coding in S1 during Discrimination of Whisker Vibrotactile Sequences. PLOS Biol. 2016; 14:e1002549. [PubMed: 27574970]

Morita T, Kang H, Wolfe J, Jadhav SP, Feldman DE. Psychometric curve and behavioral strategies for whisker-based texture discrimination in rats. PLoS One. 2011; 6:e20437. [PubMed: 21673811]

Mountcastle VB, Talbot WH, Sakata H, Hyvärinen J. Cortical neuronal mechanisms in flutter-vibration studied in unanesthetized monkeys. Neuronal periodicity and frequency discrimination. J Neurophysiol. 1969; 32:452–484. [PubMed: 4977839]

Niell CM, Stryker MP. Modulation of visual responses by behavioral state in mouse visual cortex. Neuron. 2010; 65:472–479. [PubMed: 20188652]

O'Connor DH, Clack NG, Huber D, Komiyama T, Myers EW, Svoboda K. Vibrissa-based object localization in head-fixed mice. J Neurosci. 2010a; 30:1947–1967. [PubMed: 20130203]

O'Connor DH, Peron SP, Huber D, Svoboda K, Connor DHO, Peron SP, Huber D, Svoboda K, O'Connor DH, Peron SP, et al. Neural activity in barrel cortex underlying vibrissa-based object localization in mice. Neuron. 2010b; 67:1048–1061. [PubMed: 20869600]

O'Connor DH, Hires SA, Guo ZV, Li N, Yu J, Sun Q-Q, Huber D, Svoboda K. Neural coding during active somatosensation revealed using illusory touch. Nat Neurosci. 2013; 16:958–965. [PubMed: 23727820]

Phillips JR, Johnson KO, Hsiao SS. Spatial pattern representation and transformation in monkey somatosensory cortex. Proc Natl Acad Sci U S A. 1988; 85:1317–1321. [PubMed: 3422492]

Qian J, Hastie T, Friedman J, Tibshirani R, Simon N. Glmnet for Matlab. 2013

Quist BW, Hartmann MJZ. Mechanical signals at the base of a rat vibrissa: the effect of intrinsic vibrissa curvature and implications for tactile exploration. J Neurophysiol. 2012; 107:2298–2312. [PubMed: 22298834]

Ritt JT, Andermann ML, Moore CI. Embodied information processing: vibrissa mechanics and texture features shape micromotions in actively sensing rats. Neuron. 2008; 57:599– 613. [PubMed: 18304488]

Safaai H, von Heimendahl M, Sorando JM, Diamond ME, Maravall M. Coordinated Population Activity Underlying Texture Discrimination in Rat Barrel Cortex. J Neurosci. 2013; 33:5843–5855. [PubMed: 23536096]

Schwarz C. The Slip Hypothesis: Tactile Perception and its Neuronal Bases. Trends Neurosci. 2016; 39:449–462. [PubMed: 27311927]

Severson KS, Xu D, Van de Loo M, Bai L, Ginty DD, O'Connor DH. Active Touch and Self-Motion Encoding by Merkel Cell-Associated Afferents. Neuron. 2017:1–11.

Siegle JH, Pritchett DL, Moore CI. Gamma-range synchronization of fast-spiking interneurons can enhance detection of tactile stimuli. Nat Neurosci. 2014; 17:1371–1379. [PubMed: 25151266]

Sofroniew NJ, Cohen JD, Lee aK, Svoboda K. Natural Whisker-Guided Behavior by Head-Fixed Mice in Tactile Virtual Reality. J Neurosci. 2014; 34:9537–9550. [PubMed: 25031397]

Stanislaw H, Todorov N. Calculation of signal detection theory measures. Behav Res Methods, Instruments, {&} Comput. 1999; 31:137–149.

Wallach A, Bagdasarian K, Ahissar E. On-going computation of whisking phase by mechanoreceptors. Nat Neurosci. 2016; 19:487–493. [PubMed: 26780508]

Weber AI, Saal HP, Lieber JD, Cheng J-W, Manfredi LR, Dammann JF, Bensmaia SJ. Spatial and temporal codes mediate the tactile perception of natural textures. Proc Natl Acad Sci. 2013; 110:17107–17112. [PubMed: 24082087]

Wolfe J, Hill DN, Pahlavan S, Drew PJ, Kleinfeld D, Feldman DE. Texture coding in the rat whisker system: slip-stick versus differential resonance. PLoS Biol. 2008; 6:e215. [PubMed: 18752354]

Zuo Y, Perkon I, Diamond ME. Whisking and whisker kinematics during a texture classification task. Philos Trans R Soc L B Biol Sci. 2011; 366:3058–3069.

Zuo Y, Safaai H, Notaro G, Mazzoni A, Panzeri S, Diamond ME. Complementary contributions of spike timing and spike rate to perceptual decisions in rat S1 and S2 cortex. Curr Biol. 2015; 25:357–363. [PubMed: 25619766]

Highlights

- Neural coding of surface features was studied during active whisker discrimination
- Stick-slip whisker motion events encode both local surface features and texture
- Neurons that encode local surface features also encode overall roughness
- A subset of neurons are selective for tactile grating spatial frequency

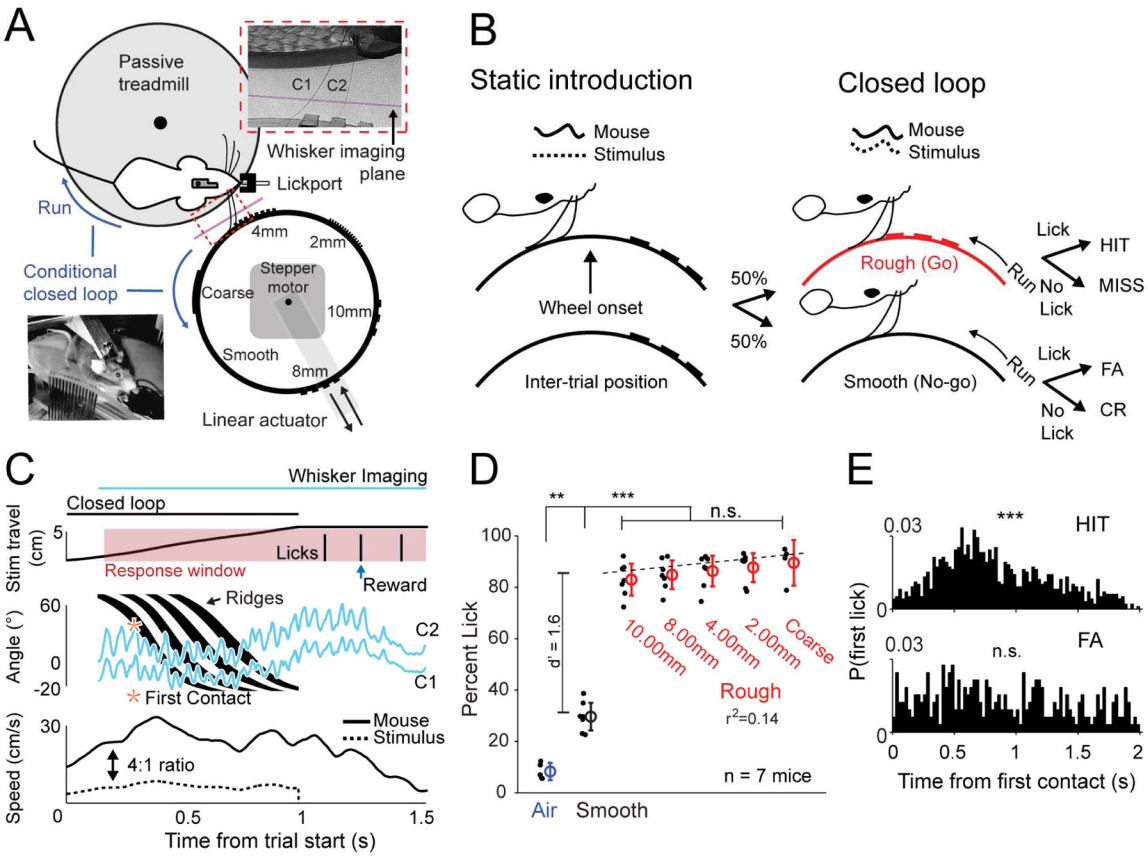

Figure 1. Discrimination of smooth vs. rough surfaces in a virtual tactile foraging task

(A) Training apparatus. A head-fixed mouse ran on a disk while a rotating stimulus cylinder presented smooth (No-go) or rough (Go) stimulus patches to the whisker field. Rough stimuli were raised ridge gratings of 2, 4, 8 and 10 mm spatial period, and a coarse (P150) sandpaper, mounted on smooth cylinder. “Smooth,” indicates segment used for Smooth trials. Top inset, video frame showing C1 and C2 whiskers contacting a ridged surface. Bottom, mouse performing the task. (B) Trial structure. Prior to each trial, the stimulus cylinder was translated to within reach of the whiskers while presenting a static (non-rotating) smooth surface. At trial onset, the stimulus wheel began to rotate closed-loop with run velocity, bringing either a Rough or Smooth patch into the whisking field. (C) An example Rough stimulus (Go) trial. Top, stimulus position and mouse licks. Middle, C1 and C2 whisker position from whisker imaging (blue) and ridge position (black) as a function of trial time. Star shows time and location of first whisker contact onto a ridge, calculated post hoc from whisker tracking (“First Contact”). Bottom, mouse run speed and stimulus velocity. (D) Behavioral performance for 7 mice. Lick rate on Smooth trials is the FA rate (ANOVA and post-hoc paired t-test). (E) Distribution of first lick times (15 ms bins) for Hit and FA trials (χ^2 goodness of fit, d.f.=79). In this and all figures, n.s. = $p > 0.05$, * $p < 0.05$, ** $p < 0.01$, *** $p < 0.001$. See also: Figure S1 and S2.

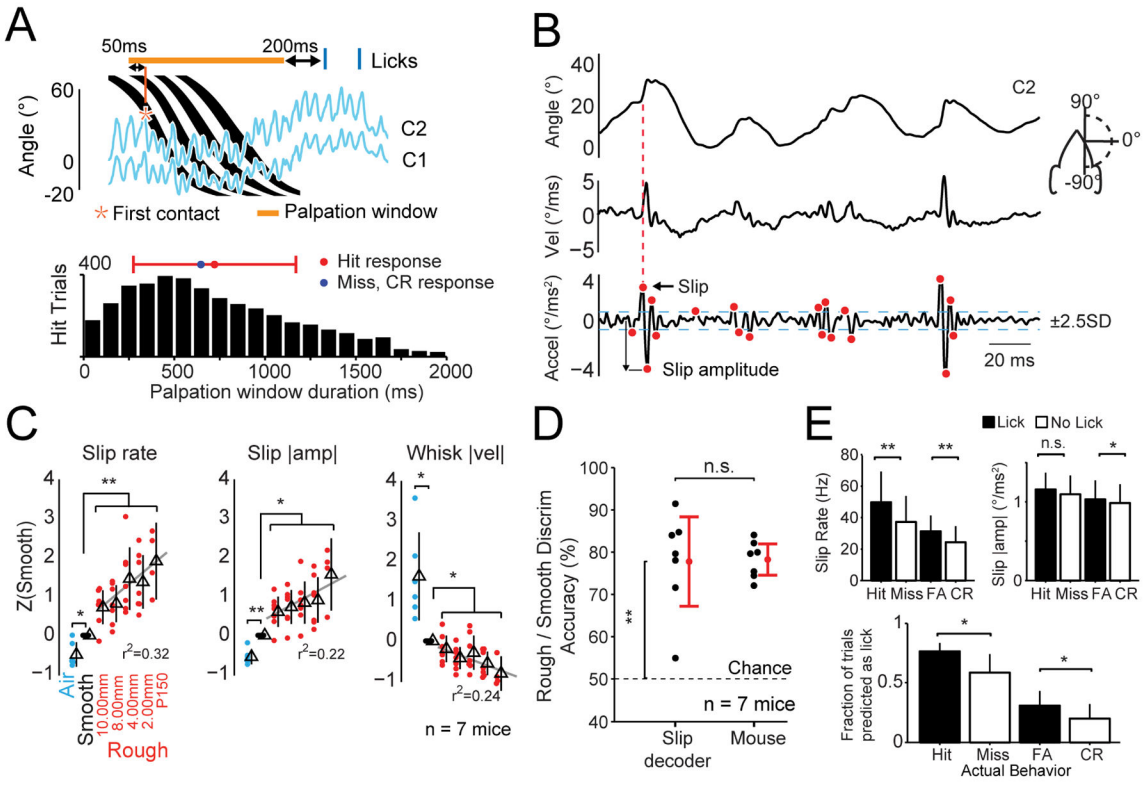

Figure 2. Slip events are a potential cue for rough surfaces

(A) Identification of palpation window for analysis of whisker slips. Bottom: Distribution of palpation window durations from Hit trials. Red is mean ±SD. Blue dot, 650 ms duration used for Miss and Correct Rejection (CR) trials. (B) C2 whisker position, velocity and acceleration for one trial. Red dots, slips with amplitude exceeding ±2.5 SD from mean. (C) Mean slip rate, slip |amplitude|, and whisker speed (|vel|) during the palpation window, z-scored to Smooth for each animal. Each point is one mouse, averaged over C1 and C2 whiskers (one-way ANOVA and post-hoc paired t-test of indicated group means). Lines show significant fits of z-score vs. spatial frequency. X-values, arbitrary units with uniform spacing. (D) Discrimination accuracy of a Rough-Smooth stimulus classifier based on C1 and C2 whisker slip rate and |amp|. Each point shows model accuracy after training on data from 1 mouse (n= 7 mice, 7,284 imaged trials). Mouse behavioral accuracy is shown for the same trials. Dashed line, chance performance (one-sample t-test). (E) Top, Mean C2 slip rate and slip |amp| for different trial types. Bottom, performance of GLM trained to predict lick or no-lick behavioral responses from whisker slip data (paired t-test, n=7 mice). Error bars represent mean ± CI_{95}; Dunn–Šidák corrections for multiple comparisons. See also: Figure S2.

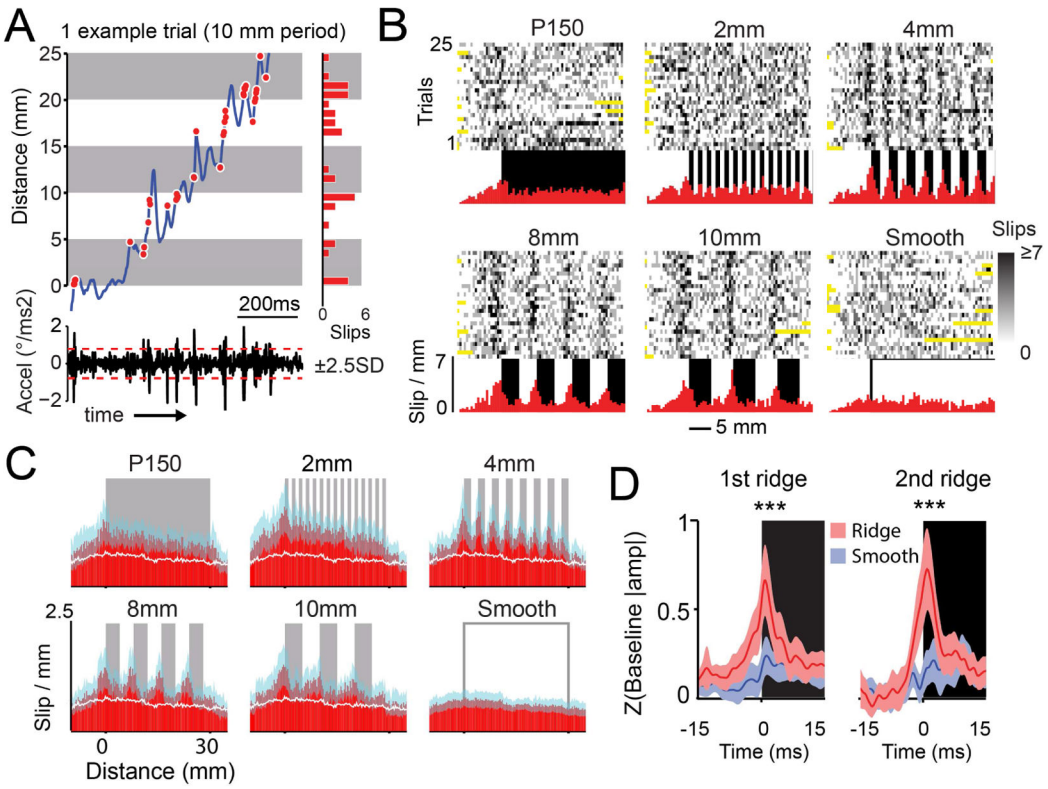

Figure 3. Slips cluster on stimulus ridges

(A) C2 whisker position (top) and acceleration (bottom) during a single trial on the 10 mm grating. Red dots, slips. Gray bars, ridges. Right: spatial histogram of slips on this trial. (B) Spatial density of slips (gray scale) for all trials on one example day. Yellow, unsampled positions. Red, mean spatial histogram across 25 trials. Black bars, ridge or sandpaper position. (C) Mean spatial histogram of slips across all imaging sessions (n=29 sessions, 7 mice). Blue, $\pm CI_{95}$. White, Smooth mean reproduced on Rough stimuli. (D) Mean $\pm$ CI_{95} ridge-triggered acceleration |amp| for the C2 whisker across first and second ridges (ANOVA, df = 119, n = 28 sessions in 6 mice). Blue, fictive ridges on Smooth cylinder. Traces z-scored to a 30 ms baseline preceding ridge-crossing. See also: Figure S3.

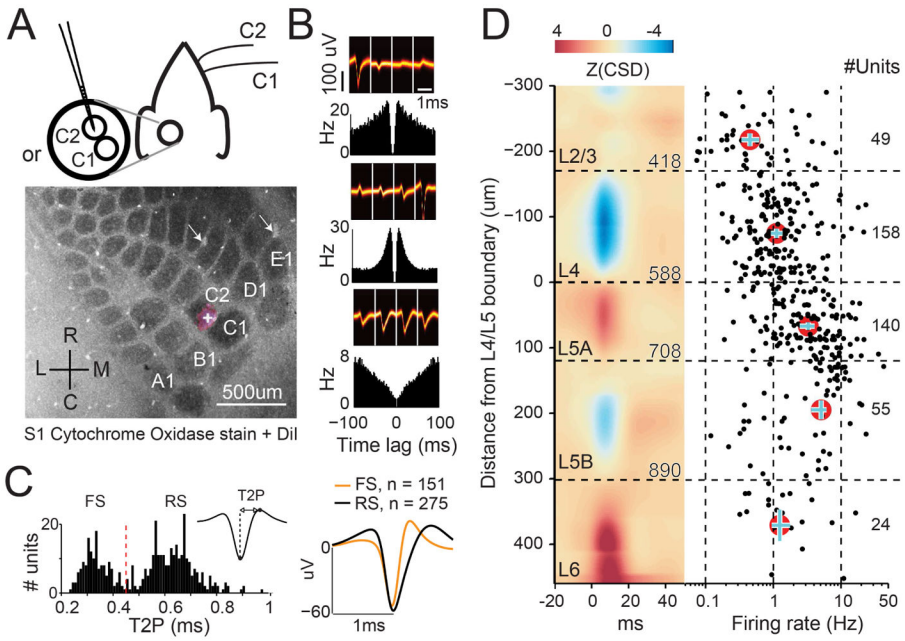

Figure 4. Extracellular single units recorded in S1

(A) Neural recording schematic and example recording site recovered in the C2 column. White cross on pink, DiI fluorescence in the C2 barrel of L4. Arrows, fiducial marks. (B) 3 example units isolated from one recording site. Spike waveforms are shown as 2D histograms of voltage on four adjacent electrode sites. Auto-correlation of spike times is shown for each unit. (C) Left: Histogram of trough-to-peak time (T2P; inset) for all units. FS-RS threshold was 0.45 ms (red dashed line). Right, mean spike waveform of identified FS and RS units. (D) Mean CSD and distribution of unit depths across all recordings. Left, mean z-scored slip-evoked CSD (n=15 recordings, 5 mice). CSDs were aligned in depth to the L4 sink - L5A source boundary. The depth from pia (microns) for each layer is shown on the CSD (Lefort et al., 2009). Right: depth and mean firing rate for each unit (black dots, n = 426). Units per layer inset at right. For each layer, mean depth and median firing rate are shown by the red circle, with bootstrapped ± CI_{95} in blue. See also: Figure S4.

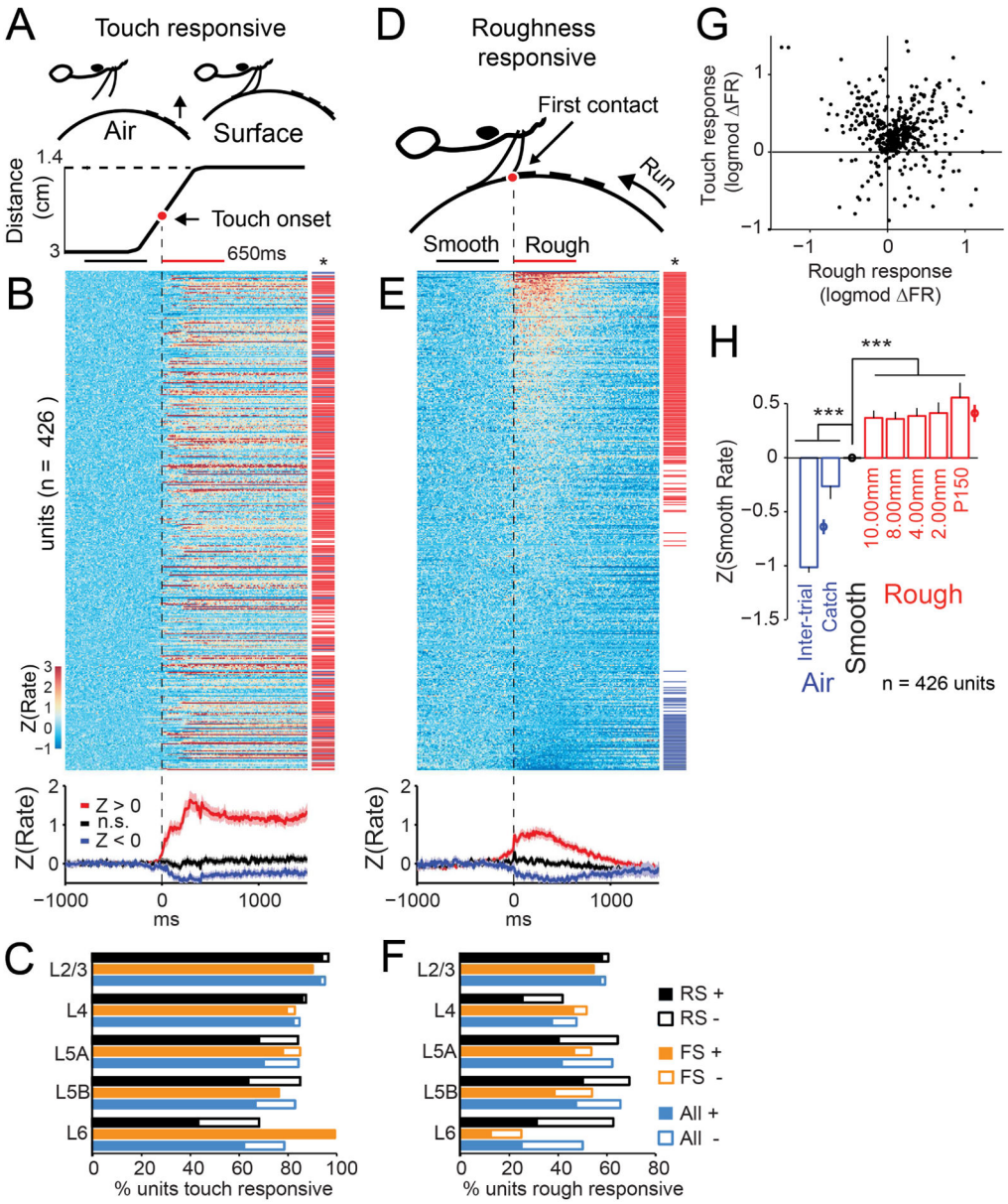

Figure 5. S1 coding of whisker touch and surface roughness

(A–C) Analysis of touch responses from static stimulus cylinder onset before trials. (A) Definition of touch onset time during static cylinder presentation (see text). Black and red bars are time windows for analysis of spiking before and after touch onset. (B) Mean spiking of each unit to touch (n = 426, 5 mice), z-scored to its firing rate in Air (zPSTHs). Right, touch-excited cells are marked in red, touch-inhibited cells in blue. White, no modulation (paired t-test of firing rate before and after contact, $\alpha = 0.05$). Bottom: mean $\pm CI_{95}$ zPSTH for touch-excited (red), touch-inhibited (blue), and non-touch-modulated neurons (black). (C) Percent of FS, RS, and all units in each layer showing significant touch responses. +, touch-excited. −, touch-inhibited. (D–F) Analysis of responses to roughness onset. (D) Schematic of time and position of first contact, with spiking analysis window before (black) and after (red) rough stimulus onset. (E) Same as (B) but for roughness onset, with

responses z-scored to smooth firing rate baseline. Units are sorted by roughness-response, and matched by row in (E) and (B). (F) same as (C) but for percent rough-responsive. (G) Relationship between firing rate response to touch and to roughness for each unit. Log-modulus firing rate change from baseline is plotted (n = 426 units, STAR Methods) (H) Mean ± CI_{95} firing rate in the palpation window for each behavioral trial type (Catch n= 561, Rough n= 2,447, Smooth n= 2,083) and inter-trial epochs (n= 5,688), z-scored to each unit's firing rate during Smooth trials. Circles show mean ± CI_{95} for Air (blue), Smooth (black), and combined Rough trials (red) ($p<0.001$, ANOVA with post hoc paired t-test, Dunn–Šidák correction for multiple comparisons). See also: Figure S5.

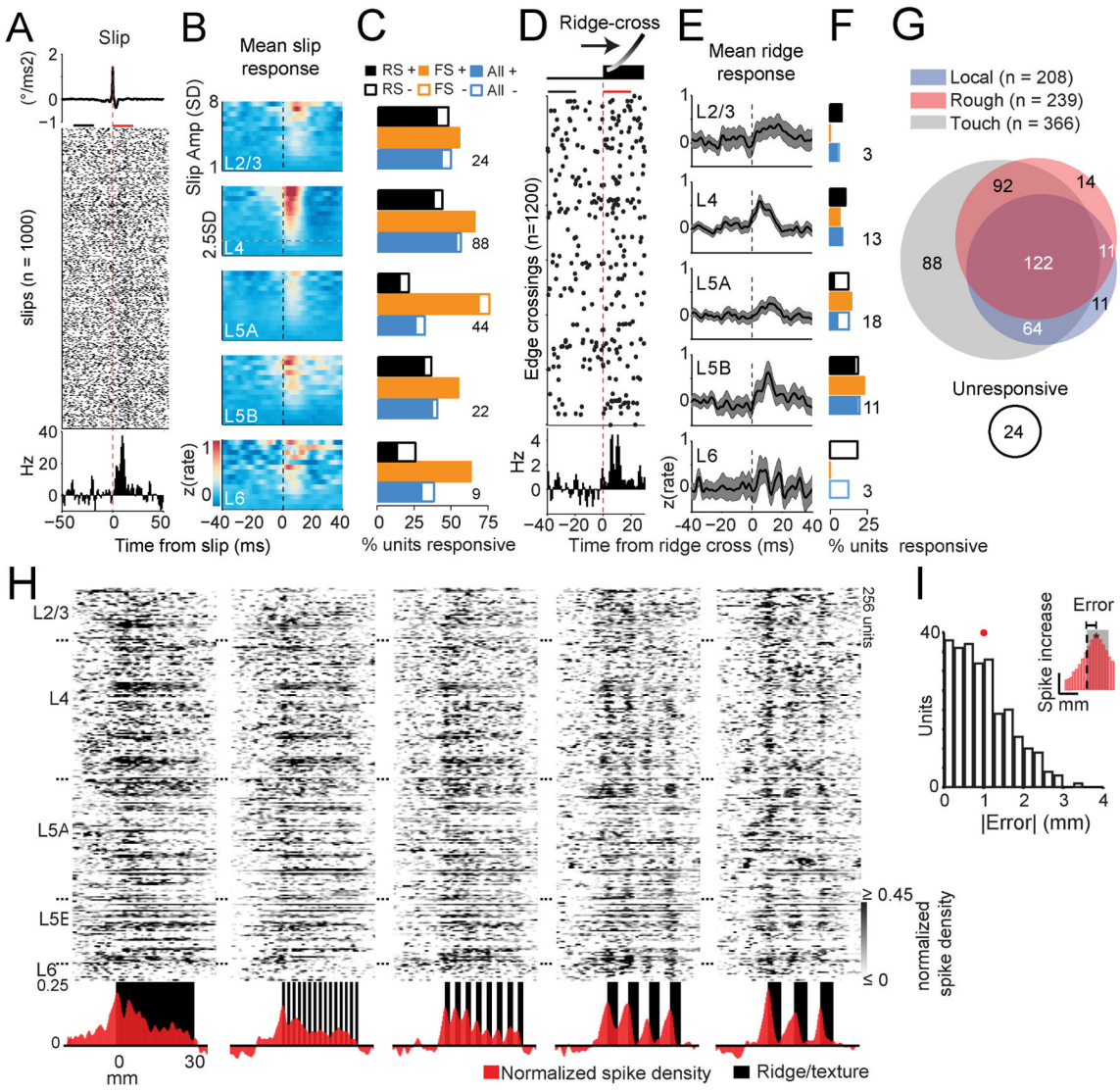

Figure 6. S1 coding of slips and ridges

(A) Slip-locked spikes for an example L4 FS unit recorded in the C1 column, shown as a raster relative to the mean C1 whisker slip event (top). Bottom, baseline-subtracted slip-locked PSTH for this unit. (B) Mean slip-locked zPSTH as a function of slip amplitude in each layer. Within each layer, each row is the mean zPSTH across all neurons (n=426) for a different slip amplitude (1–8 SD in 0.5 SD bins), z-scored to a 20 ms pre-slip baseline. Red dashed line, 2.5 SD slip threshold for slip analyses. (C) Percent of FS, RS, and all units in each layer found to be slip-sensitive (SS). +, slip-excited. −, slip-inhibited. Numbers show total number of SS units per layer. (D–F) Same as (A–C) but for ridges. (D) Spike raster for an example RS L5B unit in C2 column aligned to ridge crossing. (E) Average ridge-locked zPSTHs for each layer for all units (n = 426). PSTHs were z-scored to the pre-ridge baseline period (black bar in D). (F) same as (C) but for ridge-sensitive (RDS) units. (G) Venn diagram of unit responsiveness overlap. Blue, local features (SS + RDS). Gray, touch. Red, roughness. Numbers indicate unique units (total = 426 units). (H) Spike count increase

relative to smooth for each unit recorded in the C2 column (n=256). Units are sorted by depth (dashed line layer boundaries) and grayscale shows normalized spike density (STAR Methods). X-axis is spatial position of the whisker on stimulus cylinder, relative to first ridge position. Bottom: Median increase across units shown above vs. position of bars or sandpaper patch (black). (I) Distance of first ridge to peak in spike increase (inset) from units in (H) (mean ± SD in red, n= 255 peaks). See also: Figure S6.

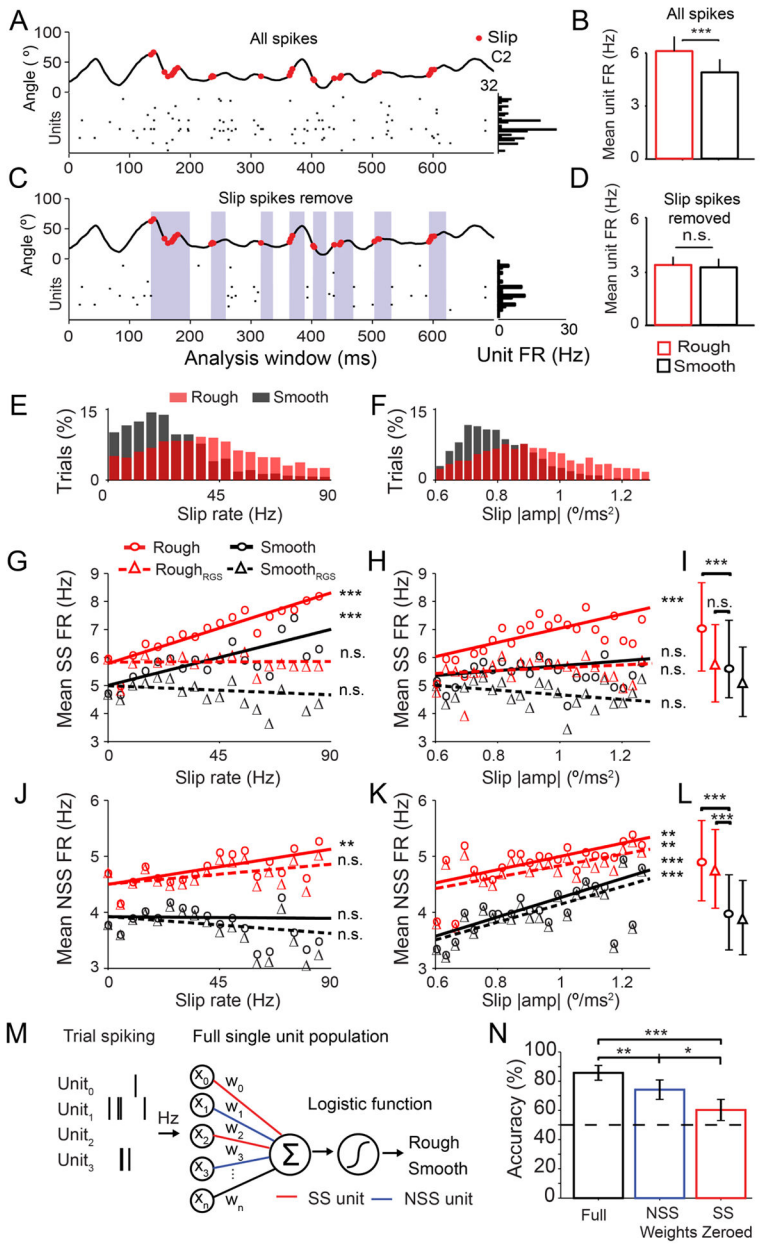

Figure 7. Slip-related spikes for coding Smooth and Rough stimuli

(A) Spiking of 32 units recorded in the C2 column on one trial with the 8 mm Rough stimulus, relative to C2 whisker motion. Red dots, slips. Right, mean firing rate of each unit during the 700-ms analysis window. (B) Mean firing rate (FR) per unit on Rough and Smooth trials (paired t-test, n = 426 units, 15 recording sessions). (C) Same trial as in (A) after slip spike removal. Purple, 20 ms windows after each slip. (D) Mean unit firing rate after procedure in (C) (paired ttest). (E–F) Distribution of Rough and Smooth trials binned by slip rate (E) or slip amplitude (F). (G) Mean unit firing rate vs. mean trial slip rate in SS units (n = 187). Weighted linear fits with significant slope indicated. Triangles with dashed line, firing rates after regressing out slip spikes ($Rough_{RGS}$ and $Smooth_{RGS}$). (H) Same as (G), but plotted as a function of mean slip amplitude (0.03 °/ms^2 bins). (I) Mean SS unit

firing rate in Rough, Smooth and slip-spike regressed trial conditions (paired t-test). (J–L) Same as (G–I) but for NSS units (n = 239). (M) Single unit population decoding model. X, mean trial firing rate from each unit used to predict Rough and Smooth stimuli. W, model coefficients weighting unit FR. (N) Single trial accuracy of decoding models before and after zeroing unit weights (one-way ANOVA with post-hoc paired t-tests). Full, mean model accuracy with no weights zeroed. NSS and SS, mean model accuracy with NSS or SS unit coefficients set to zero, respectively (STAR Methods). NSS bootstrapped to match number of SS units in each recording (possible in n= 13 recordings in 5 mice). Dunn-Šidák correction for multiple comparisons. See also: Figure S7 and Figure S8.

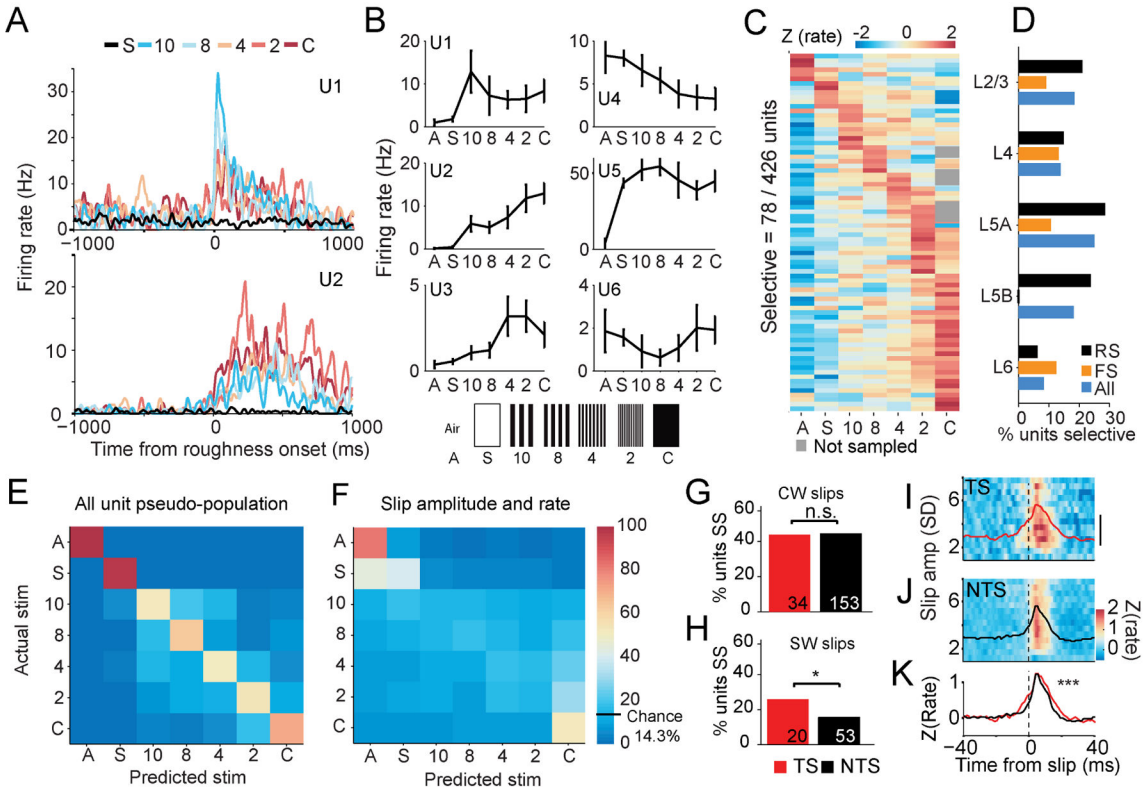

Figure 8. Discrimination between Rough stimuli in S1

(A) Two example L5A RS units with selectivity among Rough stimuli. Traces are PSTHs aligned to first contact of ridge or sandpaper, or to equivalent stimulus position on Smooth. S, Smooth. 10, 8, 4, 2 are ridge stimuli. C, coarse sandpaper. (B) Spatial frequency tuning curves for 6 L4 and L5A selective units (mean ± CI_{95}). A, Air Catch trials. U1 and U2 from (A). U5, FS from C1 column, all others RS from C2 column. (C) Mean z-scored firing rate for all stimuli for all selective units. Units are sorted by maximum stimulus response. (D) Percentage of RS, FS and all units in each layer that were stimulus selective. (E) Confusion matrix of neural decoder accuracy in classifying specific stimuli based on S1 firing rate of units combined in one pseudo-population. (F) Same as (E) but using C1 and C2 slip rate and amplitude on each session. (G) Proportion of texture selective (TS) and not texture selective (NTS) units that significantly responded to columnar whisker (CW) slips (z-test of proportions). Number of units in each category inset (H) Same as (G) for surround whisker slips (SW). (I) Mean unit CW and SW slip rate response across slip amplitudes in TS units, z-scored to baseline firing as in Figure 6B. Black line, amplitudes averaged to create mean trace overlay. (J) Same as (I) for NTS units. (K) Mean traces compared for TS and NTS units (multi-sample ANOVA, df = 78).